Electron Super-Rich Radicals in the Gas Phase. A Neutralization−Reionization Mass Spectrometric and ab Initio/RRKM Study of Diaminohydroxymethyl and Triaminomethyl Radicals

Changtong Hao, Jennifer L. Seymour, and František Tureček*

Department of Chemistry, Bagley Hall, Box 351700, University of Washington, Seattle, Washington 98195-1700

Received: April 13, 2007; In Final Form: July 3, 2007

Diaminohydroxymethyl (**1**) and triaminomethyl (**2**) radicals were generated by femtosecond collisional electron transfer to their corresponding cations ($\mathbf{1}^+$ and $\mathbf{2}^+$, respectively) and characterized by neutralization−reionization mass spectrometry and ab initio/RRKM calculations at correlated levels of theory up to CCSD(T)/aug-cc-pVTZ. Ion $\mathbf{1}^+$ was generated by gas-phase protonation of urea which was predicted to occur preferentially at the carbonyl oxygen with the 298 K proton affinity that was calculated as PA = 875 kJ mol^{-1}. Upon formation, radical **1** gains vibrational excitation through Franck−Condon effects and rapidly dissociates by loss of a hydrogen atom, so that no survivor ions are observed after reionization. Two conformers of **1**, *syn*-**1** and *anti*-**1**, were found computationally as local energy minima that interconverted rapidly by inversion at one of the amine groups with a <7 kJ mol^{-1} barrier. The lowest energy dissociation of radical **1** was loss of the hydroxyl hydrogen atom from *anti*-**1** with E_{TS} = 65 kJ mol^{-1}. The other dissociation pathways of **1** were a hydroxyl hydrogen migration to an amine group followed by dissociation to $H_2N{-}C{=}O^{\bullet}$ and NH_3. Ion $\mathbf{2}^+$ was generated by protonation of gas-phase guanidine with a PA = 985 kJ mol^{-1}. Electron transfer to $\mathbf{2}^+$ was accompanied by large Franck−Condon effects that caused complete dissociation of radical **2** by loss of an H atom on the experimental time scale of 4 μs. Radicals **1** and **2** were calculated to have extremely low ionization energies, 4.75 and 4.29 eV, respectively, which belong to the lowest among organic molecules and bracket the ionization energy of atomic potassium (4.34 eV). The stabilities of amino group containing methyl radicals, $^{\bullet}CH_2NH_2$, $^{\bullet}CH(NH_2)_2$, and **2**, were calculated from isodesmic hydrogen atom exchange with methane. The π-donating NH_2 groups were found to increase the stability of the substituted methyl radicals, but the stabilities did not correlate with the radical ionization energies.

Introduction

The electronic properties and stabilities of carbon-centered radicals are affected by the presence of electron-donating and electron-withdrawing groups bound to the carbon atom. The effects of σ-withdrawing (F, CF_3), π-withdrawing (NO_2, C═O, CN), and π-donating groups (NH_2, OH, etc.) have been studied experimentally and computationally with the aim of relating the stability and electronic properties of these radicals to the nature of the substituents.[1−8] Of much interest have also been combined (captodative) effects of π-electron donors and π-electron attractors in multifunctional carbon-centered radicals.[6] Recently, carbon-centered radicals carrying amino groups have become of interest in connection with electron-transfer,[9] electron−ion,[10] and ion−ion recombination reactions[11] in the gas phase in which α-amino alkyl radicals are thought to play an important role.[12−16]

Experimental studies of functionalized carbon-centered radicals have mostly relied on generating these transient species in the gas phase by femtosecond electron transfer to the corresponding cations or by collisional electron detachment from gas-phase anions. We and others have used this approach to generate several radicals and study their stability and unimolecular dissociations in an isolated state in the rarefied gas phase, as reviewed recently.[9] One feature that distinguishes carbon radicals having π-electron donors from similar closed-shell molecules is their low electron binding energies, as quantitatively expressed by very low adiabatic ionization energies. This led Lossing and co-workers to label α-aminoalkyl radicals "organic alkali metals" because their ionization energies (IEs) were below those of lithium and sodium.[3,8] However, the series of extremely electron-rich radicals have so far not been extended by preparing and studying radicals in which multiple amino groups would be placed on a single carbon atom. We now report a combined experimental and computational study of diaminohydroxymethyl ($(H_2N)_2C^{\bullet}{-}OH$, **1**) and triaminomethyl radicals ($(H_2N)_3C^{\bullet}$, **2**).

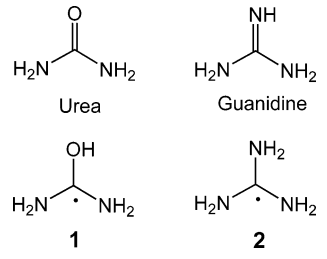

We wish to show that these species definitely qualify as organic alkali metals by having ionization energies that are comparable to that of atomic potassium (4.34 eV).[17]

Radicals **1** and **2** are hydrogen atom adducts to urea and guanidine, respectively, and their chemical properties thus have a bearing on the chemistry of those stable molecules, as well. Urea has a special place in chemistry because it was the first organic molecule synthesized by chemical means from cyanic

10.1021/jp072903l CCC: $37.00
Published on Web 08/17/2007

acid and ammonia by the German chemist Friedrich Wöhler.[18] Urea is also one of the simplest known biologically relevant molecules. The reactivity of urea has been thoroughly studied by experimental and theoretical methods.[19−26] For example, thermal decomposition of urea produces isocyanic acid and ammonia. However, the thermochemical properties and reactivity of urea radicals are unknown. Previous studies also addressed the protonation of urea,[27−30] its gas-phase basicity,[31,32] and structure.[33] Guanidine is known as a strong organic base ($pK_B = 0.4$ in water),[34] but to our knowledge its unimolecular gas-phase chemistry has not been explored.[35] In this paper, we report an experimental and computational study of radicals **1** and **2** and their respective isotopomers, $(H_2N)_2C^{\bullet}-OD$ (**1**-d_1), $(D_2N)_2C^{\bullet}-OH$ (**1**-d_4), $(D_2N)_2C^{\bullet}-OD$ (**1**-d_5), and $(D_2N)_3C^{\bullet}$ (**2**-d_6).

Experimental Section

Materials. Urea, *N*-ethylurea, guanidine carbonate, dimethyl disulfide (DMDS; all Sigma-Aldrich), and ammonia (Scott Specialty Gas Inc.) were used as received. D_2O (99.9% D), acetone-d_6 (99.9% D), and ammonia-d_3 (99.9% D), all Cambridge Isotope Laboratories, were used as received. Urea-d_4 was prepared by H/D exchange as follows. Urea (0.5 g) was dissolved in 1.5 mL of D_2O and stirred for 5 h. The solvent was evaporated in vacuo, and the solid was used for measurements. Guanidine-d_6 carbonate was prepared as follows. Guanidine carbonate (0.5 g) was dissolved in 1.0 mL of D_2O and stirred for 24 h. The solvent was evaporated in vacuo, and the solid was used for measurements.

Methods. Neutralization−reionization mass spectra were measured on the University of Washington tandem quadrupole acceleration−deceleration mass spectrometer described previously.[36] Cations were generated in electron impact (EI) or chemical ionization (CI) ion sources.[37] Typical ionization conditions were as follows: emission current 500 μA for electron impact and 1 mA for chemical ionization. The electron energy was tuned for the best signal but typically was 70 eV for the EI source and 100 eV for the CI source. The source temperature was 200−240 °C. Urea was introduced into the ion source from a glass direct probe at the ion source temperature. Ammonia (NH_3), ammonia-d_3 (ND_3), acetone, and acetone-d_6 were used as CI reagent gases at pressures of $(1.0-1.7) \times 10^{-4}$ Torr as read on an ionization gauge located at the diffusion pump intake. Precursor cations were extracted from the ion source and passed through a quadrupole mass filter operated in the radio-frequency-only mode, accelerated to a total kinetic energy of 7170 eV, and neutralized in the collision cell floated at −7170 V. Dimethyl disulfide (DMDS) was introduced to the differentially pumped collision cell at a pressure to achieve 70% transmittance of the precursor ion beam. The ions and neutrals were allowed to drift to a four-segment conduit, where the ions were reflected by the first segment floated at +250 V. The neutral drift time through the conduit was 4.0−4.1 μs for **1** through **2**-d_6. The fast neutral species were reionized in the second collision cell with oxygen at a pressure to achieve 70% transmission of the precursor ion beam. The ions formed in the second collision cell were decelerated, the fast neutrals were blocked by a chicane lens that also provided an ion kinetic energy filter, and the ions passing the filter were analyzed by a second quadrupole mass filter operated at unit mass resolution. The decelerating potential and the quadrupole mass filter were scanned in a linked fashion to transmit ions of a selected mass and kinetic energy. The kinetic energy bandwidth was ∼40 eV. Typical spectra consisted of 50−100 accumulated repetitive scans. The instrument was tuned daily to maximize the ion current of reionized $CS_2^{+\bullet}$.

Collisionally activated dissociation (CAD) spectra of $\mathbf{1}^+$ and its isotopomers were measured on a JEOL HX-110 double-focusing mass spectrometer of forward geometry (the electrostatic sector E precedes the magnet B). Collisions with air were monitored in the first field-free region at a pressure in 70% transmittance of the ion beam at 10 keV. The spectra were obtained by scanning E and B simultaneously while maintaining a constant B/E ratio (B/E linked scan).

Calculations. Standard ab initio calculations were performed using the Gaussian 03 suite of programs.[38] Geometries for ions, neutral molecules, radicals, and transition states were optimized with Becke's hybrid functional (B3LYP)[39] and the 6-31+G-(d,p) basis set. Because of the electron-rich nature of the radical species, the urea-derived radicals were also optimized with B3LYP using the larger 6-311++G(2d,p) basis set that includes diffuse functions on hydrogen atoms. The optimized structures were characterized by harmonic frequency analysis as local minima (all frequency real) or first-order saddle points (one imaginary frequency). Zero-point vibrational energies (ZPVE) were calculated from B3LYP/6-31+G(d,p) frequencies, which were scaled by 0.963.[40] The B3LYP/6-311++G(2d,p) frequencies were scaled by 0.981. The rigid-rotor harmonic oscillator approximation was used in all thermochemical calculations. The B3LYP-optimized geometries were used for single-point energy calculations using MP2 and B3LYP and the larger 6-311+G-(3df,2p), 6-311++G(3df,2p), and Dunning's correlation-consistent triple-ζ basis set augmented with polarization and diffuse functions on all the atoms, aug-cc-pVTZ.[41] Spin-unrestricted calculations (UB3LYP and UMP2) were used for open-shell systems. In the UB3LYP and UMP2 calculations, $\langle S^2 \rangle$ operator expectations values ranged from 0.75 to 0.76 and from 0.75 to 0.78 for the local minima and transition-state structures, respectively, indicating low spin contamination. Quadratic configuration interaction[42] and coupled clusters[43] with single, double, and disconnected triple excitations of valence electrons (QCISD(T) and CCSD(T))[44] with the 6-31++G(d,p) and 6-311G(d,p) split valence basis sets were performed to treat electron correlation in both valence and diffuse orbital shells.[45] The single-point calculations were expanded to include the larger 6-311+G(3df,2p) and 6-311++G(3df,2p) basis sets using the standard linear formula (1):

$$E[\text{CCSD(T)/large basis set}] \cong E[\text{CCSD(T)/small basis set}] + E[\text{MP2/large basis set}] - E[\text{MP2/small basis set}] \quad (1)$$

In addition, single-point calculations were performed with CCSD(T) and the large aug-cc-pVTZ basis set for selected local energy minima and transition states. The single-point energies obtained on the B3LYP/6-31+G(d,p)- and 6-311++G(2d,p)-optimized geometries were within 0.3 mhartree (0.8 kJ mol^{-1}) for all species under study and were considered equivalent at the present levels of theory. Dissociation pathways were investigated by changing one internal coordinate in 0.05−0.1 Å steps while fully optimizing the other internal coordinates.

Franck−Condon energies in vertical neutralization and reionization were taken as absolute differences between the B3-PMP2 or CCSD(T) energies of fully optimized ion and neutral structures and those in which an electron has been added to an optimized cation structure or subtracted from an optimized neutral structure. No zero-point corrections were applied to the calculated Franck−Condon energies. Excited electronic states were addressed by time-dependent density functional theory calculations[46] using B3LYP and the aug-cc-pVTZ basis set.

SCHEME 1

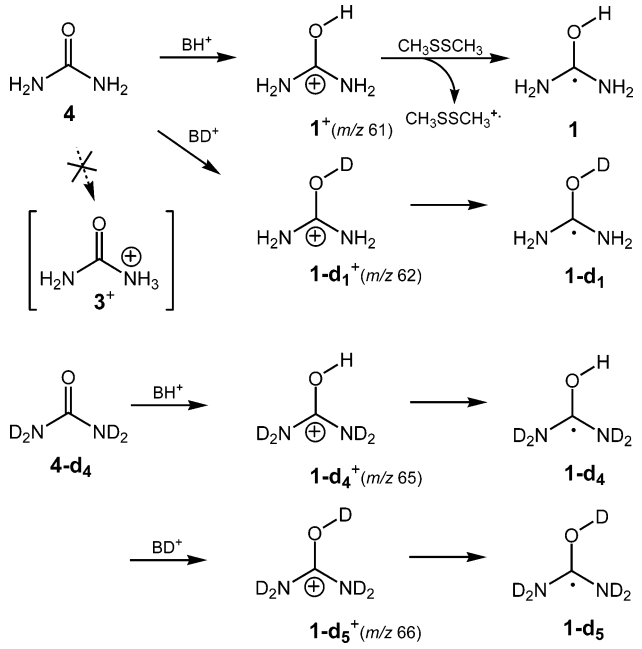

Selected excited-state geometries were optimized by configuration interaction singles (CIS)[47] using the 6-311++G(2d,p) basis set.

Unimolecular rate constants were calculated by the Rice−Ramsperger−Kassel−Marcus (RRKM) theory[48] using Hase's program[49] that was recompiled for Windows XP.[50] The RRKM rate constants were obtained by direct count of quantum states at internal energies that were increased in 2 kJ mol^{-1} steps from the transition state up to 200 kJ mol^{-1} above the reactant. Rotations were treated adiabatically, and the calculated $k(E,J,K)$ microscopic rate constants were Boltzmann-averaged over the thermal distribution of rotational states at 473 K, corresponding to the ion source temperature, to provide canonical rate constants $k(E)$.

Results and Discussion

Urea Cations and Radicals. Cations $\mathbf{1}^+$ through $\mathbf{1}$-d_5^+ were prepared by gas-phase protonation of urea (**4**) and its isotopomers in a standard chemical ionization source (Scheme 1; BH^+ and BD^+ indicate generic gas-phase acids). Ammonia and acetone were used as CI gases to produce NH_4^+ and $(CH_3)_2C{-}OH^+$, respectively, which protonated urea to give rise to ion $\mathbf{1}^+$ (m/z 61). The $(H_2N)_2C{-}OD^+$ cation ($\mathbf{1}$-d_1^+, m/z 62) was generated from urea under nonexchanging conditions of acetone-d_6/$(CD_3)_2C{-}OD^+$-CI. Likewise, $(D_2N)_2C{-}OH^+$ ($\mathbf{1}$-d_4^+, m/z 65) was prepared from urea-d_4 with acetone/$(CH_3)_2C{-}OH^+$-CI. The fully deuterated cation $(D_2N)_2C{-}OD^+$ ($\mathbf{1}$-d_5^+, m/z 66) was prepared from urea-d_4 under exchanging conditions of ND_3/ND_4^+-CI.

The probable structures of gas-phase ions $\mathbf{1}^+{-}\mathbf{1}$-$d_5^+$ were established on the basis of ion stabilities obtained from calculations of topical proton affinities (PAs) and gas-phase basicities (GBs) in urea at several levels of theory up to CCSD(T)/aug-cc-pVTZ (Table 1).

Gas-phase urea was found to exist as two practically isoenergetic isomers, a C_2 structure **4**(C_2) and a C_s structure **4**(C_s) (Figure 1), such that their enthalpy and free energy differences were $\Delta H^\circ_{g,298}\{\mathbf{4}(C_2) \rightarrow \mathbf{4}(C_s)\} = 3.4$ kJ mol^{-1} and $\Delta G^\circ_{g,298}\{\mathbf{4}(C_2) \rightarrow \mathbf{4}(C_s)\} = 1.1$ kJ mol^{-1}. Protonation at the carbonyl oxygen atom in **4**(C_2) forming ion $\mathbf{1}^+$ (PA = 875 kJ mol^{-1}, GB = 848 kJ mol^{-1}) was substantially more favorable than protonation at one of the nitrogen atoms forming ion $\mathbf{3}^+$ (Scheme 1, PA = 814 kJ mol^{-1}). The reaction enthalpy in gas-phase proton transfer to urea from NH_4^+ ($-\Delta H^\circ_{rxn,298} = 875-853 = 22$ kJ mol^{-1}) and $(CH_3)_2C{-}OH^+$ ($-\Delta H^\circ_{rxn,298} = 875-802 = 73$ kJ mol^{-1}) was likely to be dissipated by multiple collisions that the ions underwent in the high-pressure CI-ion source. The internal energy of $\mathbf{1}^+$ was estimated to be $E_{int} = 24$ kJ mol^{-1} at a gas-phase equilibrium at 500 K.

Note on the Proton Affinity of Urea. The topical proton affinities reported here are consistent with previous experimental[27,31] and theoretical[28,29] studies of urea protonation sites in the gas and condensed phases.[30,33] Interestingly, though, a recently revised value of the proton affinity of urea, determined from competitive ion dissociations of proton-bound dimers (the kinetic method) as PA = 868 ± 2.5 kJ mol^{-1},[32] was lower than the previous estimate from the same laboratory and by a similar method (PA = 873 kJ mol^{-1}),[31] so that the revised value is now in less satisfactory agreement with the values calculated at high levels of theory. To obtain the proton affinity, Zheng and Cooks reported their estimate of protonation entropy of urea as 9.4 ± 0.5 J mol^{-1} K^{-1},[32] which is in good but fortuitous agreement with the 298 K value calculated by standard thermodynamics for the reaction $\mathbf{1}^+ \rightarrow \mathbf{4}(C_2) + H^+$ ($\Delta S_{g,298} = 9.3$ J mol^{-1} K^{-1}). However, since **4**(C_2) and **4**(C_s) coexist as a 60:40 mixture at 298 K, both must be formed in proton-transfer reactions used by Zheng and Cooks to estimate the reaction thermochemistry. This introduces an additional entropy of mixing term for the products, $S_{mix} = -R[x(C_2)\ln x(C_2) + x(C_s)\ln x(C_s)]$, where $x(C_2)$ and $x(C_s)$ are the pertinent molar fractions of **4**(C_2) and **4**(C_s), respectively. The correction to the measured proton affinity, PA = GB + $T(S_{mix} + \Delta S_{g,298})$, depends on the "effective temperature" of the previous measurements where the TS_{mix} term ranges from 2.8 at 500 K to 8.4 at 1500 K. Hence, including the entropy of mixing would bring the experimental estimate of the proton affinity of urea closer to the calculated value.

The calculated proton affinities were further used to assess the performance of the various levels of theory in comparison with the benchmark CCSD(T)/aug-cc-pVTZ single-point calculations. The data in Table 1 show that the energies from the B3-MP2 and composite QCISD(T) and CCSD(T) calculations were within 3−4 kJ mol^{-1} of the benchmark data and thus were deemed to be reliable for the studies of the more challenging open-shell radical systems.

Ion Dissociations of $\mathbf{1}^+$. Metastable ion and collisionally activated dissociations (CAD) of cation $\mathbf{1}^+$ (m/z 61) showed the formation of H_2NCO^+ (m/z 44) as the major channel (Table 2). The elimination of ammonia mainly involved the hydroxyl and amine hydrogen atoms to form the NH_2CO^+ ion. However, the CAD spectra indicated that a fraction of the precursor ions underwent intramolecular H/D exchange between the OH and NH_2 groups upon excitation, as evidenced by the elimination of NH_3 from $\mathbf{1}$-d_1^+ and ND_3 from $\mathbf{1}$-d_4^+ (Table 1). The elimination of ammonia showed isotope effects that disfavored deuteron transfers from the OD group in $\mathbf{1}$-d_1^+ and from the ND_2 group in $\mathbf{1}$-d_5^+ (Table 2). The elimination of ammonia was calculated to require 213 kJ mol^{-1} at the thermochemical threshold (Table 3). Ion $\mathbf{3}^+$, which is a likely intermediate in the loss of NH_3, shows a substantially elongated $C{-}NH_3$ bond (Scheme 2). The transition state separating $\mathbf{1}^+$ and $\mathbf{3}^+$ was calculated at 180 kJ mol^{-1} above $\mathbf{1}^+$, which was below the dissociation threshold (Table 3). This indicates that $\mathbf{1}^+$ and $\mathbf{3}^+$ can interconvert at internal energies exceeding that of the

TABLE 1: Proton Affinities and Ionization Energies in Urea and Guanidine

	urea[a]			guanidine		
	PA[b]			PA[b]		
method	C=*O*[c]	C(*N*H$_2$)[c]	IE$_{adiab}$[d]	C=*N*H[c]	C(*N*H$_2$)[c]	IE$_{adiab}$[d]
B3LYP/6-31+G(d,p)	875	811	9.56	997	848	8.34
B3LYP/6-311+G(3df,2p)	879	812	9.58	997	846	8.37
B3LYP/6-311++G(3df,2p)	879	812	9.58	997	846	8.37
B3LYP/aug-cc-pVTZ	881	813	9.57	998	847	8.37
MP2/6-31++G(d,p)	865	814	9.97	986	849	8.36
MP2/6-311G(d,p)	886	837	9.76	1001	867	8.22
MP2/6-311+G(3df,2p)	863	806	10.18	980	838	8.59
MP2/6-311++G(3df,2p)	863	806	10.18	980	838	8.59
MP2/aug-cc-pVTZ	866	808	10.22	978	839	8.65
B3-MP2/6-311+G(3df,2p)[e]	871	809	9.88 (10.32)[g]	989	842	8.48 (9.26)[g]
B3-MP2/6-311++G(3df,2p)[e]	871	809	9.88 (10.32)[g]	989	842	8.48
B3-MP2/aug-cc-pVTZ[e]	873	810	9.90 (10.33)[g]	988	843	8.51
CCSD(T)/6-31++G(d,p)	875	819	9.52	991	855	8.22
QCISD(T)/6-31++G(d,p)	875	820	9.51	991	855	8.22
QCISD(T)/6-311G(d,p)	895	843	9.35	1006	873	8.09
QCISD(T)/6-311+G(3df,2p)[f]	872	813	9.77 (10.65)[g]	984	845	8.47 (9.26)[g]
QCISD(T)/6-311++G(3df,2p)[f]	874	812	9.73 (10.65)[g]	985	845	8.45 (9.25)[g]
CCSD(T)/6-311++G(3df,2p)[f]	874	812	9.73 (10.66)[g]	985	845	8.45 (9.25)[g]
CCSD(T)/aug-cc-pVTZ	875	813	9.79	985	846	8.50

[a] Relative to the more stable C_2 structure. [b] Proton affinities in kJ mol^{-1} including zero-point and 298 K enthalpy corrections. [c] Atoms in italics denote the protonation sites. [d] Adiabatic ionization energies in eV including zero-point energies and referring to 0 K. [e] Composite single-point energies: E[B3-MP2] = 0.5{E[B3LYP] + E[MP2]}. [f] Composite single-point energies: E[CCSD(T)/large basis set] ≅ E[CCSD(T)/small basis set] + E[MP2/large basis set] − E[MP2/small basis set]. [g] Vertical ionization energies in eV without zero-point corrections.

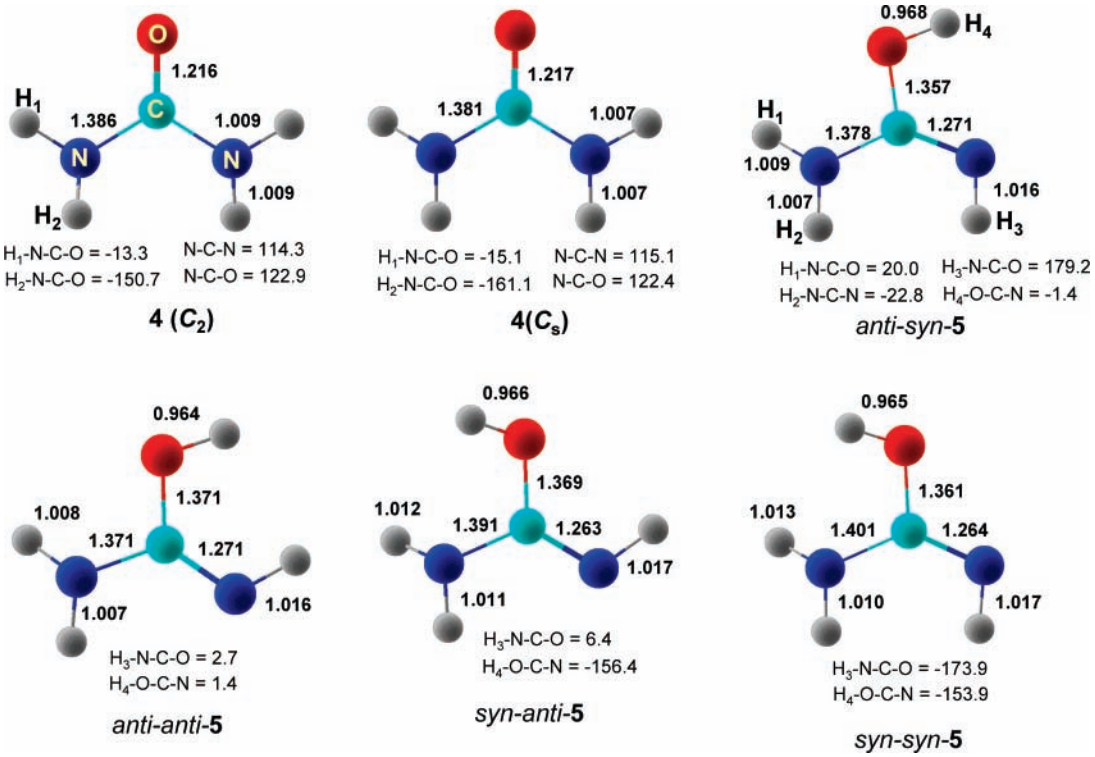

Figure 1. B3LYP-optimized structures of urea and isourea conformers **4** and **5**.

transition state for isomerization (E_{TS} = 180 kJ mol^{-1}), in keeping with the observed hydrogen exchange between the OH and NH$_2$ groups in dissociating **1**$^+$.

CAD at 10 keV of **1**$^+$ also resulted in losses of H$^\bullet$ (*m*/*z* 60) and NH$_2^\bullet$ (*m*/*z* 45), consecutive dehydrogenation of the primary fragments (*m*/*z* 43 and 42), and the formation of NH$_3^{+\bullet}$ at *m*/*z* 17. Interestingly, the loss of NH$_2^\bullet$ was not affected by hydrogen exchange between the NH$_2$ and OH groups, as corroborated by the CAD spectrum of **1**-d_4^+, which showed a peak at *m*/*z* 47 due to loss of ND$_2$ but no peak at *m*/*z* 48 due to loss of NHD. Losses of H$^\bullet$ and NH$_2^\bullet$ are high-energy dissociations that require ≥500 kJ mol^{-1} to proceed, as illustrated by the calculated dissociation thresholds for the formation of cation radicals of urea (**4**$^{+\bullet}$), isourea (**5**$^{+\bullet}$), and H$_2$N−C−OH$^{+\bullet}$ (Table 3). To be competitive with the loss of ammonia, these high-energy dissociations must originate from excited electronic states of **1**$^+$ that are accessed in collisions at kiloelectronvolt center-of-mass kinetic energies.[51]

It should be noted that the combined intensities of CAD products were less than 2% relative to the precursor ion. This indicated that the precursor ion was relatively stable upon kiloelectronvolt collisions and that ion dissociations probably

TABLE 2: Collisionally Activated Mass Spectra of 1^+, $1\text{-}d_1^+$, $1\text{-}d_4^+$, and $1\text{-}d_5^+$

	relative intensity			
m/z	$\mathbf{1}^+$	$\mathbf{1}\text{-}d_1^+$	$\mathbf{1}\text{-}d_4^+$	$\mathbf{1}\text{-}d_5^+$
66	–	–	–	*a*
65	–	–	*a*	23.1
64	–	–	16.8	–
63	–	–	14.3	–
62	–	*a*	–	–
61	*a*	33.0	–	–
60	21.5	–	–	–
48	–	–	–	11.1
47	–	–	8.9	–
46	–	9.7	44.3[b]	57.2[b]
45	8.3	29.0	17.7	–
44	43.9[b]	35.1[b]	9.4	7.4
43	10.0	15.8	–	–
42	5.2	–	–	–
33	–	–	–	11.5
32.5	–	–	10.3	–
30.5	7.3	–	–	–
30	–	–	5.4	–
22	–	–	–	5.8
20	–	–	3.9	7.0
17	3.8	–	–	–

[a] Precursor ions. [b] Fragments also present as intense metastable peaks.

TABLE 3: Ion Relative and Dissociation Energies

	relative energy[a,b]				
	B3-MP2			CCSD(T)	
reaction	A[d]	B[e]	G2(MP2)[c]	A[d]	B[e]
$\mathbf{1}^+ \rightarrow \mathbf{3}^+$	52	54	60	53	59
$\mathbf{1}^+ \rightarrow \mathbf{TS}(\mathbf{1}^+ \rightarrow \mathbf{3}^+)$	180	179	180	180	179
$\mathbf{1}^+ \rightarrow H_2NC{=}O^+ + NH_3$	208	210	209	212	213
$\mathbf{1}^+ \rightarrow \mathbf{4}^{+\bullet} + H^\bullet$	504	507	498	496	502
$\mathbf{1}^+ \rightarrow \mathbf{5}^{+\bullet} + H^\bullet$	499	501	497	496	501
$\mathbf{2}^+ \rightarrow \mathbf{8}^+$	146	145	139	141	138
$\mathbf{2}^+ \rightarrow \mathbf{TS}(\mathbf{2}^+ \rightarrow \mathbf{8}^+)(\mathbf{TS10})$	220	217	218	219	216
$\mathbf{2}^+ \rightarrow H_2NC{=}NH^+ + NH_3$	240	239	241	242	241
$\mathbf{2}^+ \rightarrow \mathbf{9}^{+\bullet} + H^\bullet$	488	490	485	484	488

[a] In units of kJ mol^{-1}. [b] Including B3LYP/6-31+G(d,p) zero-point energies and referring to 0 K. [c] Effective QCISD(T)/6-311+G(3df,2p) calculations without empirical corrections for the number of electrons.[56] [d] Calculations with the 6-311+G(3df,2p) basis set. [e] Calculations with the aug-cc-pVTZ basis set.

did not significantly contribute to the formation of neutral fragments to interfere in the neutralization−reionization spectra.

Dissociations of Radical 1. The neutralization−reionization ($^+NR^+$) mass spectrum of $\mathbf{1}^+$ showed no survivor ion at *m/z* 61 regardless of the mode of ion preparation (Figure 2). Survivor ions were also absent in the $^+NR^+$ mass spectra of ions $\mathbf{1}\text{-}d_1^+$−$\mathbf{1}\text{-}d_5^+$ (Figure 3). With regard to the substantial stability of ion $\mathbf{1}^+$, the $^+NR^+$ results imply that radical **1** was unstable on the 4 μs time scale under the conditions of vertical electron transfer. The $^+NR^+$ spectrum of $\mathbf{1}^+$ was remarkably similar to the $^+NR^+$ mass spectrum of the urea cation radical $\mathbf{4}^{+\bullet}$ that was obtained for reference (Figure 4). Both showed weak peaks of $\mathbf{4}^{+\bullet}$ at *m/z* 60 and fragments at *m/z* 44 and 43 due to loss of NH_2 and NH_3, respectively, *m/z* 29−27, *m/z* 17 ($NH_3^{+\bullet}$), and its dissociation products at *m/z* 16−14. This indicated that the primary dissociation of radical **1** was loss of a hydrogen atom forming urea (**4**) or isourea (**5**) as intermediates.

The $^+NR^+$ mass spectra of $\mathbf{1}\text{-}d_1^+$ and $\mathbf{1}\text{-}d_4^+$ showed losses of H and D in 1.3:1 and 1:1 ratios, respectively (Figure 3a,b). These distributions for H loss from the OH and NH_2 groups are nonstochastic, as statistical H/D ratios would be 4:1 and 1:4 for $\mathbf{1}\text{-}d_1$ and $\mathbf{1}\text{-}d_4$, respectively. Thus, the spectra indicated some preference for the loss of the hydroxyl hydrogen to form urea. The H loss was subject to primary ($\alpha = k_{H\alpha}/k_{D\alpha}$) and secondary ($\beta = k_{H\beta}/k_{D\beta}$) isotope effects. The $^+NR^+$ branching ratios for loss of H and D were fitted by relative rate constants for loss of H from the OH group (k_{OH}) and NH_2 groups (k_{NH_2}), and the pertinent isotope effects such that $k_{OH}/k_{NH_2} = 3.47$, $\alpha = 2.35$, and $\beta = 2.0$. These indicated that the formation of urea by loss of the OH hydrogen atom was the main channel, whereas formation of the less stable isourea by loss of one of the amino hydrogen atoms was a minor channel.

The further dissociations of urea and its cation radical $\mathbf{4}^{+\bullet}$ can be tracked in the $^+NR^+$ mass spectrum through the relative intensities of the *m/z* 44 (loss of NH_2) and *m/z* 43 (loss of NH_3) peaks and likewise for the labeled derivatives. Figure 4a shows a [*m/z* 44]/[*m/z* 43] ratio from $\mathbf{4}^{+\bullet}$ to be equal to 0.63, which was close to the same ratio in the $^+NR^+$ mass spectrum of $\mathbf{1}^+$ (0.64). However, Figure 4b shows the [*m/z* 46]/[*m/z* 44] ratio from $\mathbf{4}\text{-}d_4^{+\bullet}$ as 1.29, which was larger than the same abundance ratio in the $^+NR^+$ spectrum of $\mathbf{1}\text{-}d_5^+$ (0.64, Figure 3c). Furthermore, the latter spectrum (Figure 3c) shows a substantial peak at *m/z* 64 that was attributed to a mixture of $\mathbf{4}\text{-}d_4^{+\bullet}$ and $\mathbf{5}\text{-}d_4^{+\bullet}$. Note that the analogous survivor peak is of a much lower relative intensity in the $^+NR^+$ spectrum of $\mathbf{4}\text{-}d_4^{+\bullet}$ (Figure 4b). These differences will be discussed later in context with the energetics of radical and cation-radical dissociations. Cation radical $\mathbf{5}^{+\bullet}$, corresponding to the kinetically unstable molecule **5**,[19] was generated by dissociative ionization of *N*-ethylurea, and its $^+NR^+$ mass spectrum was measured for reference (Figure S1, Supporting Information). The $^+NR^+$ spectra of $\mathbf{4}^{+\bullet}$ and $\mathbf{5}^{+\bullet}$ were very similar and lacked unique fragments that could be used for isomer distinction.

The complementary formation of ammonia in radical and ion dissociations was compared using the $^+NR^+$ and CAD spectra of labeled urea derivatives. The $^+NR^+$ spectrum of $\mathbf{1}\text{-}d_1^+$ showed the formations of $NH_2D^{+\bullet}$ and $NH_3^{+\bullet}$ in a 0.52 ratio (Figure 3a). This was very different from the ratio for elimination of NH_2D and NH_3 from $\mathbf{1}\text{-}d_1^+$ upon CAD, which was ≅1.0 after correction for consecutive dehydrogenations. Likewise, upon $^+NR^+$ $\mathbf{1}\text{-}d_4^+$ showed the formation of ND_3 and ND_2H in a 1.86 ratio, which differed from the analogous elimination of ammonia upon CAD of the ion, which gave a ratio of 0.40. These data indicated that ammonia was produced from radical **1** either by a neutral dissociation process or following hydrogen atom loss and reionization to $\mathbf{4}^{+\bullet}$ or $\mathbf{5}^{+\bullet}$. A clue was provided by the $^+NR^+$ spectrum of $\mathbf{1}\text{-}d_4^+$ (Figure 3b). This showed a 1:1 formation of $[D_2NCOND_2]^{+\bullet}$ ($\mathbf{4}\text{-}d_4^{+\bullet}$) and $[D_2NC(OH){=}ND]^{+\bullet}$ upon loss of H and D, respectively, followed by reionization. Ion $\mathbf{4}\text{-}d_4^{+\bullet}$ can eliminate ND_2 and ND_3 only to produce fragments at *m/z* 46, 44, and 20 (Figure 4b). Ion $[D_2NC(OH){=}ND]^{+\bullet}$ can eliminate both ND_3 and ND_2H to give rise to fragments at *m/z* 43, 44 and *m/z* 20, 19. Figure 3b shows that the elimination of ND_2H is more abundant, probably due to primary isotope effects on D-atom migration.

Energetics of Urea Cation-Radical Dissociations. Urea (**4**) and isourea (**5**) were identified as the primary products of radical **1** dissociations. Structures of the ion species detected after collisional ionization are shown in Scheme 3, and the pertinent dissociation and TS energies are summarized in Table 4. Interestingly, cation radicals $\mathbf{4}^{+\bullet}$ and $\mathbf{5}^{+\bullet}$ are nearly isoenergetic, $\Delta H°_{g,0}(\mathbf{4}^{+\bullet} \rightarrow \mathbf{5}^{+\bullet}) = -1.6$ kJ mol^{-1}, and are separated by a relatively low energy barrier for isomerization by H atom migration, $E_{\mathbf{TS(45)}} = 134$ kJ mol^{-1} (Table 4). This explains the similarity between the $^+NR^+$ mass spectra of $\mathbf{4}^{+\bullet}$ and $\mathbf{5}^{+\bullet}$ (vide

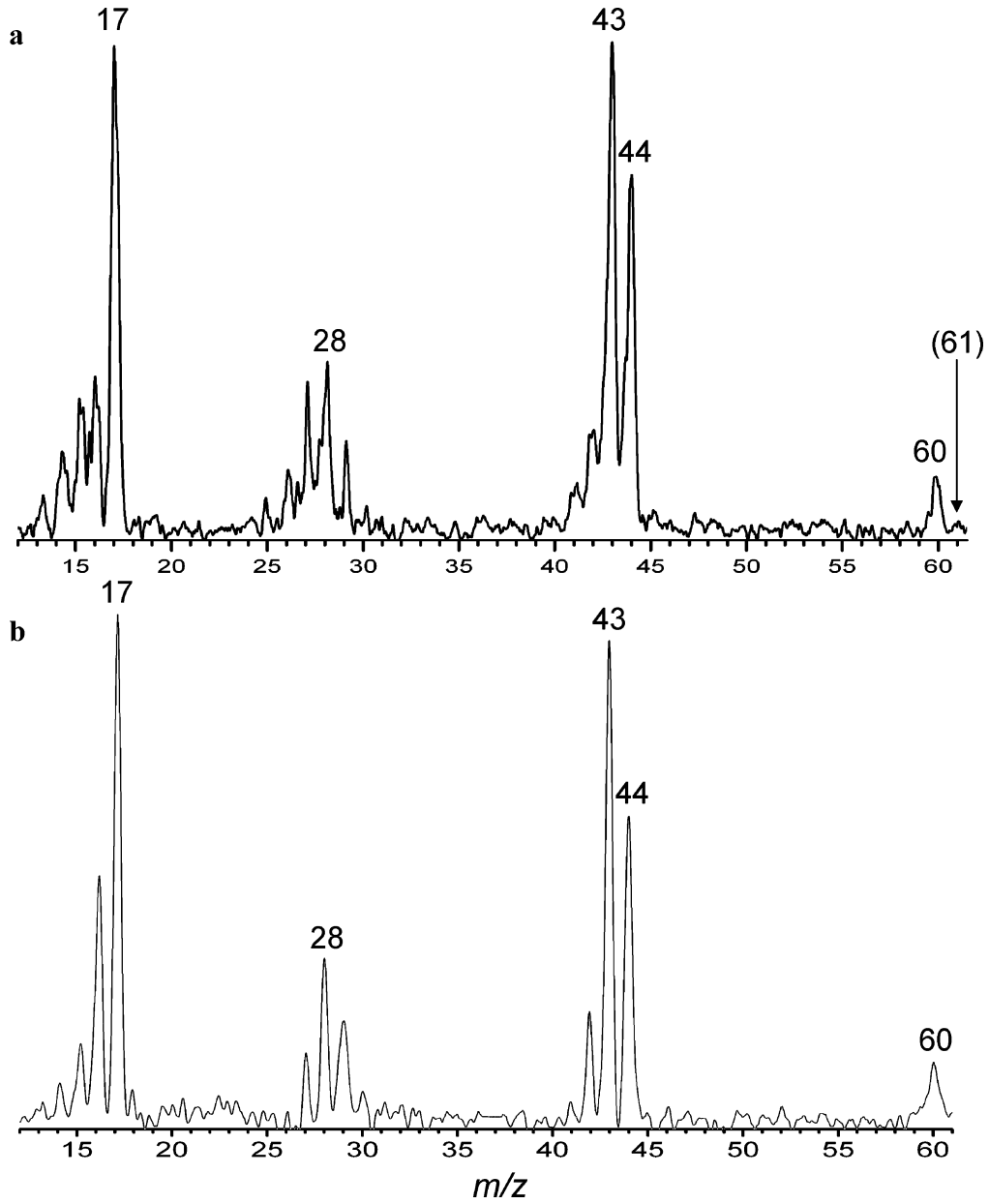

Figure 2. $^{+}NR^{+}$ mass spectra (CH_3SSCH_3, 70% transmittance/O_2, 70% transmittance) of $\mathbf{1}^{+}$ protonated with (a, top) $(CH_3)_2COH^{+}$ and (b, bottom) NH_4^{+}.

SCHEME 2

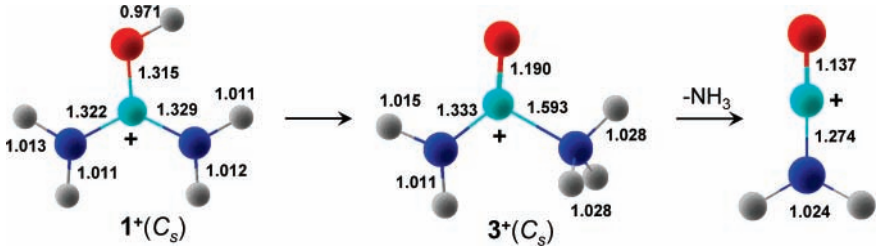

supra), as the ions can undergo fast isomerization through **TS**(**45**) prior to neutralization or following reionization.

Dissociation of $\mathbf{4}^{+\bullet}$ and $\mathbf{5}^{+\bullet}$ to $[NH_3 + HN{=}C{=}O]^{+\bullet}$ must involve H-atom migrations, e.g., through **TS**(**46**) at $E_{TS} = 194$ kJ mol^{-1} or through **TS**(**56**) at $E_{TS} = 196$ kJ mol^{-1}. The latter reaction also involves a low-energy rotation of the OH group in $\mathbf{5}^{+\bullet}$ to reach **TS**(**56**). Intermediate $\mathbf{6}^{+\bullet}$ was calculated to be 47 kJ mol^{-1} less stable than $\mathbf{4}^{+\bullet}$ and underwent further isomerization along the dissociation coordinate to form the ion-dipole complex $\mathbf{7}^{+\bullet}$. Ion $\mathbf{7}^{+\bullet}$ showed a long O−N bond between the HN=C=O and NH_3 components and a charge distribution that indicated 76% of spin and positive charge density to be in the incipient $NH_3^{+\bullet}$ fragment. This correlated with the dissociation energies of $\mathbf{7}^{+\bullet}$ that were $\Delta H^{\circ}_{g,0} = 46$ and 182 kJ mol^{-1} for the formations of $NH_3^{+\bullet} + HN{=}C{=}O$ and $HN{=}C{=}O^{+\bullet} + NH_3$, respectively. The difference in the threshold energies reflects the difference between the adiabatic ionization energies of NH_3 (10.10 eV calculated, 10.07 eV experimental)[52] and

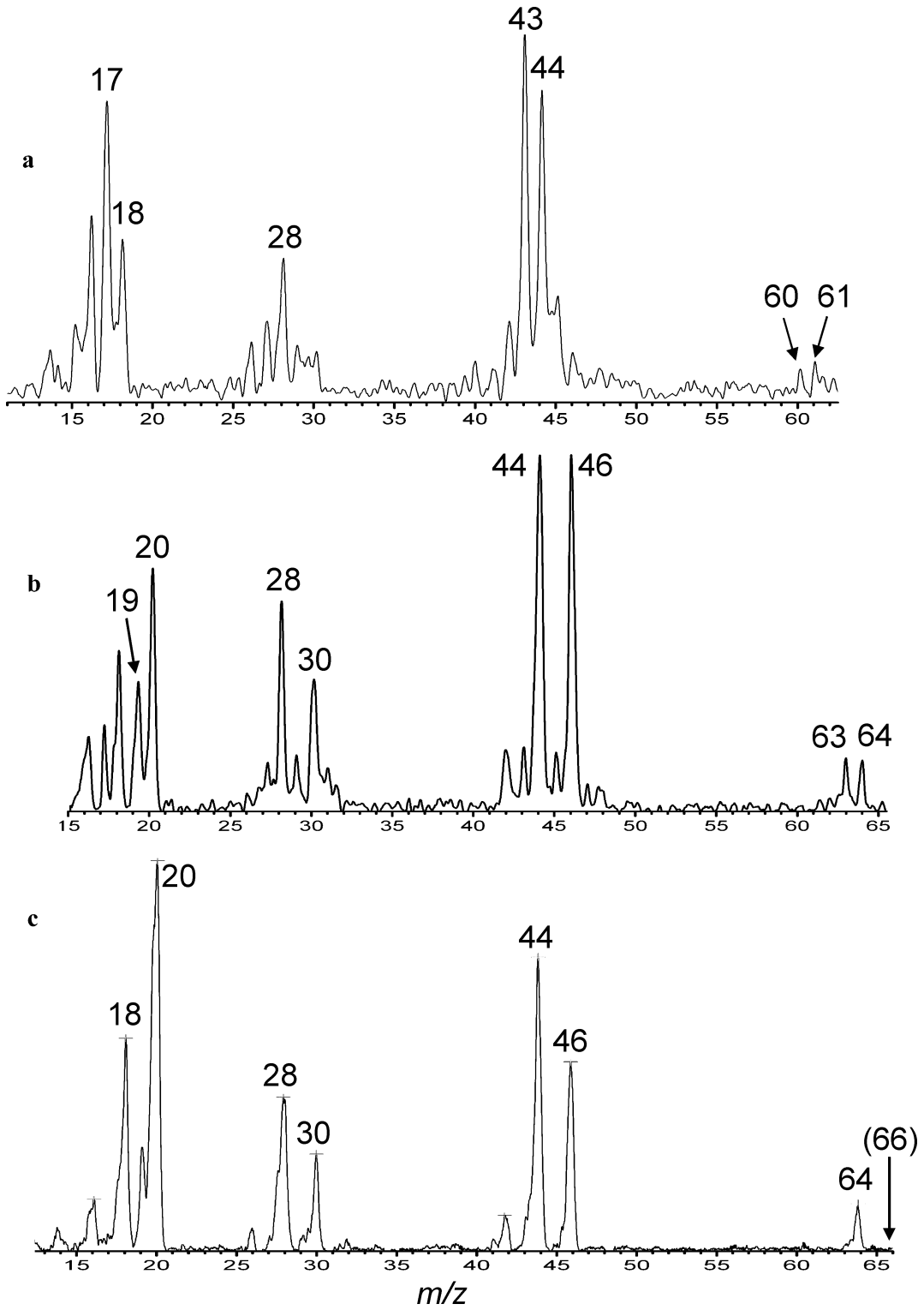

Figure 3. $^{+}NR^{+}$ mass spectra (CH_3SSCH_3, 70% transmittance/O_2, 70% transmittance) of (a) **1**-d_1^{+}, (b) **1**-d_4^{+}, and (c) **1**-d_5^{+}.

HN═C═O (11.51 eV calculated, 11.59 eV experimental).[52] The loss of NH_2 from $\mathbf{4}^{+\bullet}$ was calculated to require 146 kJ mol^{-1} threshold dissociation energy, which was lower than **TS**(**46**) on the route leading to $NH_3^{+\bullet}$. However, the dissociations of $\mathbf{4}^{+\bullet}$ showed preferential formation of $NH_3^{+\bullet}$, which indicated that the loss of NH_2 may require an additional energy barrier for the C−N bond dissociation.

Noteworthy is the low intensity of the urea and isourea survivor ions in the $^{+}NR^{+}$ mass spectra (Figures 4 and S1) in spite of the substantial stability of both neutral molecules and their cation radicals. The low stability of urea under $^{+}NR^{+}$ can be in part ascribed to the combined Franck−Condon effects in vertical electron transfer to $\mathbf{4}^{+\bullet}$ that results in 69 kJ mol^{-1} mean vibrational excitation in the urea molecules formed, and vertical ionization of relaxed urea that results in 89 kJ mol^{-1} mean vibrational excitation in ions $\mathbf{4}^{+\bullet}$. The combined Franck−Condon energies can drive ion dissociations of a high-energy-tail population of $\mathbf{4}^{+\bullet}$. In addition, excited electronic states of urea, when formed by vertical electron transfer to $\mathbf{4}^{+\bullet}$, may undergo dissociation to NH_3 and HN═C═O, which was observed by Duvernay et al. as a major dissociation channel upon VUV irradiation of urea in a frozen xenon matrix.[19]

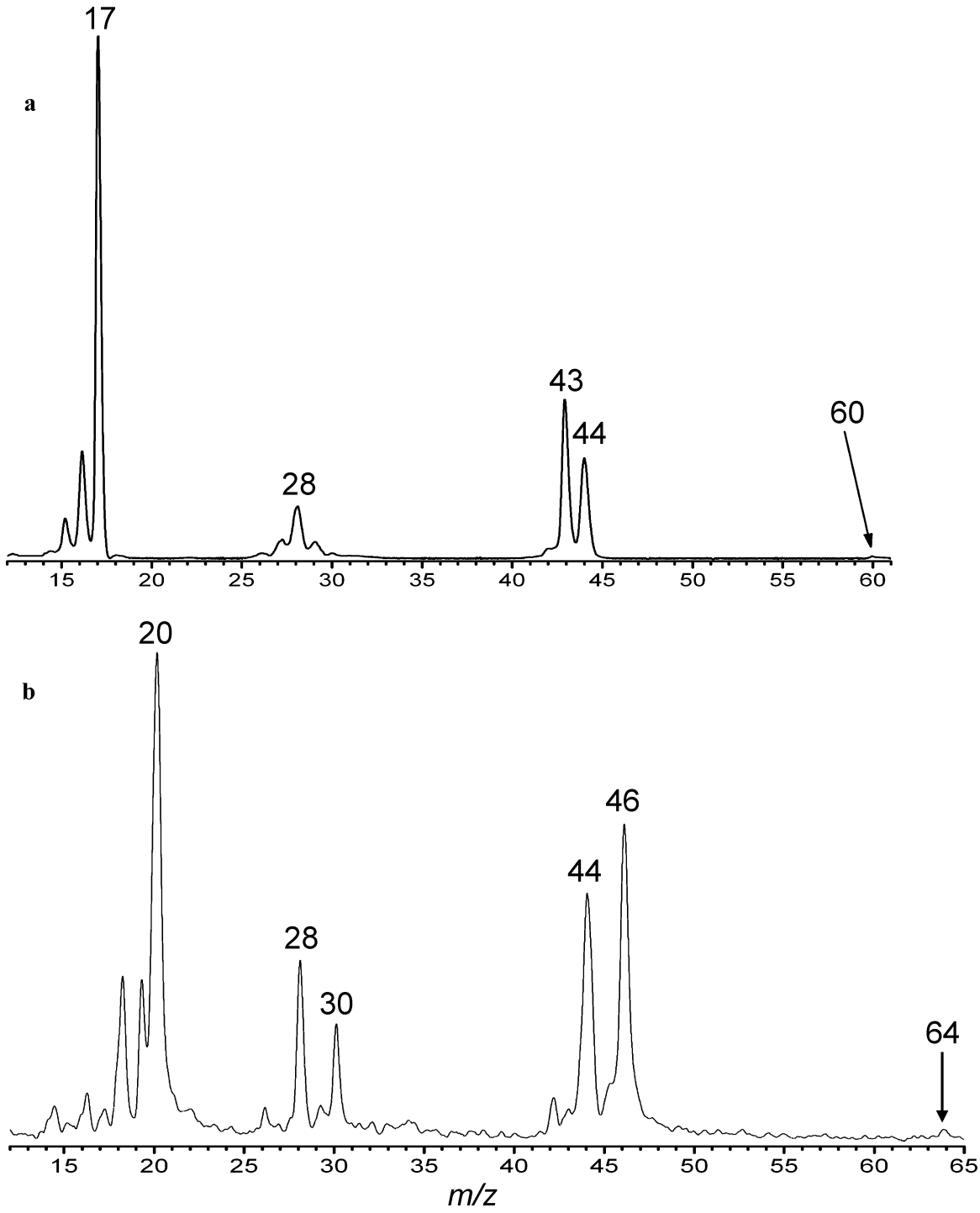

Figure 4. $^{+}NR^{+}$ mass spectra (CH_3SSCH_3, 70% transmittance/O_2, 70% transmittance) of (a) $\mathbf{4}^{+\bullet}$ and (b) $\mathbf{4}$-$d_4^{+\bullet}$.

Duvernay et al. concluded that the formation of NH_3 and HNCO occurred on the triplet (T_1) excited electronic state of urea. We note that triplet states are directly accessible by electron transfer to the ground doublet state of $\mathbf{4}^{+\bullet}$, and the T_1 state may be kinetically significant for promoting dissociations because of its long radiative lifetime. We did not distinguish the dissociations of neutral urea and its cation radical in the present study; note, however, that dissociations originating from excited electronic states played a significant role in collisional neutralization of uracil, which is a cyclic urea derivative.[53]

Energetics and Kinetics of Urea Radical Dissociations. Geometry optimization found two conformers as local energy minima for radical **1** that differed in the OH and NH_2 group orientation. The more stable *syn*-**1** (Figure 5) is pyramidized at C and in both NH_2 groups and shows a favorable orientation of the N−H and O−H bond dipoles with respect to the lone electron pairs at the opposite NH_2 groups. The other isomer, *anti*-**1**, also shows substantial pyramidization at C and NH_2, but its O−H bond is in an anti orientation to the lone electron pairs at both NH_2 groups (Figure 5). Radicals *syn*-**1** and *anti*-**1** are connected by a low-lying transition state (**TS1**) for an umbrella inversion at N-3 (Figure S2, Supporting Information), as confirmed by vibrational analysis of the pertinent mode in **TS1** ($\nu = 462\text{i}\ \text{cm}^{-1}$). The pyramidization in *syn*-**1** and *anti*-**1** and other differences from the precursor cation $\mathbf{1}^{+}$ geometry result in substantial Franck−Condon effects upon vertical

SCHEME 3

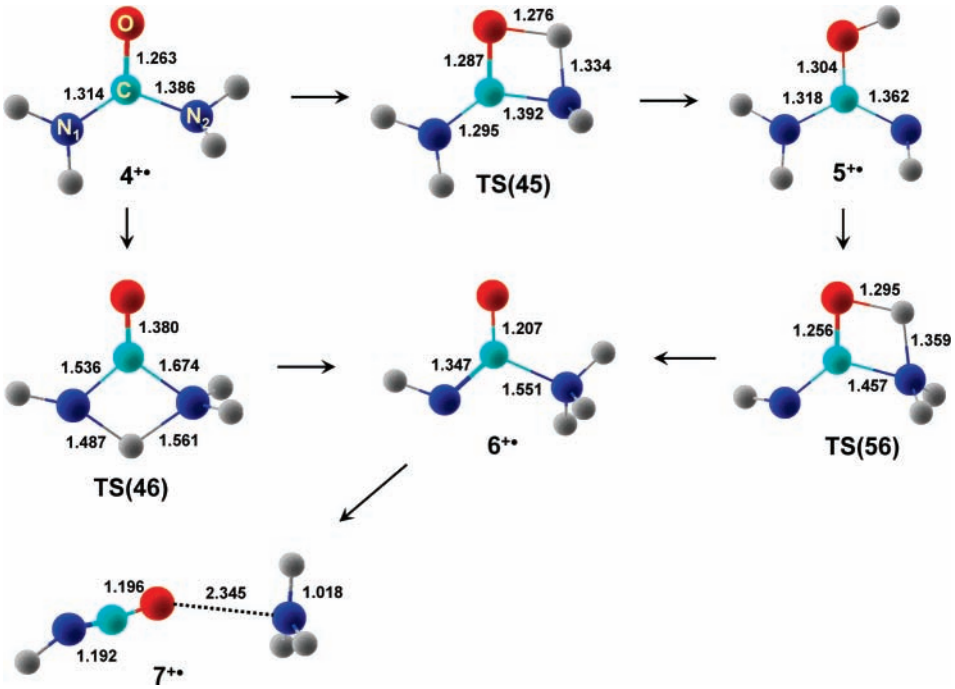

TABLE 4: Cation Radical Relative and Dissociation Energies

	energy[a,b]				
			B3-PMP2		
reaction	B3LYP/ 6-31+G(d,p)	G2(MP2)[c]	A[d]	B[e]	CCSD(T) B[e]
4 → **4**$^{+\bullet}$	923	943	954	955	944 (9.79)[f]
E_{FC}(**4**→**4**$^{+\bullet}$)[g]		85	42	42	89
E_{FC}(**4**$^{+\bullet}$→**4**)[g]		68	67	67	69
5 → **5**$^{+\bullet}$	872	879	883	885	883 (9.15)[f]
E_{FC}(**5**→**5**$^{+\bullet}$)[g]		47	43	42	
4$^{+\bullet}$ → **5**$^{+\bullet}$	18	−1.3	−5.4	−6.3	−1.6
TS(45)	145	131	121	121	134
TS(46)	203	195	191	190	194
TS(56)	194	197	197	194	196
4$^{+\bullet}$ → **6**$^{+\bullet}$	68	45	49	49	47
4$^{+\bullet}$ → **7**$^{+\bullet}$	42	35	16	17	40
4$^{+\bullet}$ → NH_3 + HN=C=O$^{+\bullet}$	262	223	222	222	229
4$^{+\bullet}$ → $NH_3^{+\bullet}$ + HN=C=O	120	88	79	79	93
4$^{+\bullet}$ → H_2N=C=O$^+$ + $NH_2^\bullet$	183	144	138	138	146
9$^{+\bullet}$ → HN=C−NH_2^+ + $NH_2^\bullet$	202	189	186	185	189
9$^{+\bullet}$ → HN=C=$NH^{+\bullet}$ + NH_3	238	231	228	228	233
9$^{+\bullet}$ → NC≡$NH_2^{+\bullet}$ + NH_3	256	250	253	252	250

[a] In units of kJ mol^{-1}. [b] Including B3LYP zero-point energies and referring to 0 K. [c] Effective QCISD(T)/6-311+G(3df,2p) calculations without empirical corrections for the number of electrons.[56] [d] Single-point calculations with the 6-311+G(3df,2p) basis set. [e] Single-point calculations with the aug-cc-pVTZ basis set. [f] Adiabatic ionization energies in eV. [g] Franck−Condon energies in vertical ionization or electron attachment.

electron transfer, as documented by the 87 kJ mol^{-1} difference between the vertically formed and optimized structures of *syn*-**1**.

The dissociation and TS energies for **1** that were calculated at several levels of theory are summarized in Table 5 and displayed in Figure 6. The lowest energy dissociation of *syn*-**1** and *anti*-**1** is dissociation of the O−H bond proceeding through distinct transition states, **TS2** and **TS3**, respectively (Figure S2, Supporting Information). The higher energy **TS2** connects *syn*-**1** with **4**(C_s) while the slightly lower energy **TS3** connects *anti*-**1** with **4**(C_2), as confirmed by intrinsic reaction coordinate analysis of both pathways. The overall dissociation by O−H bond cleavage was 19−21 kJ mol^{-1} endothermic to form the urea isomers. Interestingly, the activation energies for the reverse H-atom additions to **4**(C_2) and **4**(C_s) are practically identical at 54 kJ mol^{-1}.

Due to the presence of three asymmetric centers in *syn*-**1** and *anti*-**1**, dissociations of the N−H bonds can proceed through 2^3 = 8 different pathways to convergently form the four rotamers of isourea, e.g., *syn-syn*-**5**, *anti-syn*-**5**, *syn-anti*-**5**, and *anti-anti*-**5** (Figure 1). Out of these, *anti-syn*-**5** is the most stable rotamer due to the favorable orientation of the O−H and N−H dipoles in the essentially planar molecule. The syn orientation of the O−H bond in *syn-anti*-**5** and *syn-syn*-**5** is destabilizing and results in a 24−27° out-of-plane twist of the OH group (Figure 1). The TSs for the N−H bond dissociations in *syn*-**1** and *anti*-**1** correlate with the product stabilities, such that **TS4** and **TS5** leading to *anti-syn*-**5** require the least energies (Table 5). Nevertheless, **TS4** and **TS5** are 26−28 kJ mol^{-1} above **TS2** and **TS3**.

Elimination of ammonia from *syn*-**1** and *anti*-**1** is 27−31 kJ mol^{-1} exothermic, making the radicals metastable with respect to this dissociation. The elimination proceeds through a single transition state (**TS6**) which shows an elongated C−NH_3 bond at 1.655 Å (Figure S2, Supporting Information). The **TS6** energy (E_{TS} = 138 kJ mol^{-1}) indicates that the loss of ammonia cannot be expected to compete with the more favorable loss of H through **TS2** and **TS3** on the same potential energy surface of the ground electronic state in *syn*-**1** and *anti*-**1**. However, it should be noted that if **TS6** was crossed, the H_2N−C=O$^\bullet$ product would have sufficient energy to undergo consecutive dissociation to $NH_2^\bullet$ and CO through **TS9** (Figure 6). Other possible pathways to elimination of ammonia are by H-atom migration between the amino groups in *syn*-**1** and *anti*-**1**. Figure 6 shows that these pathways require high-energy transition states (**TS7** and **TS8**) which make the loss of ammonia unlikely to be competitive on the ground-state potential energy surface.

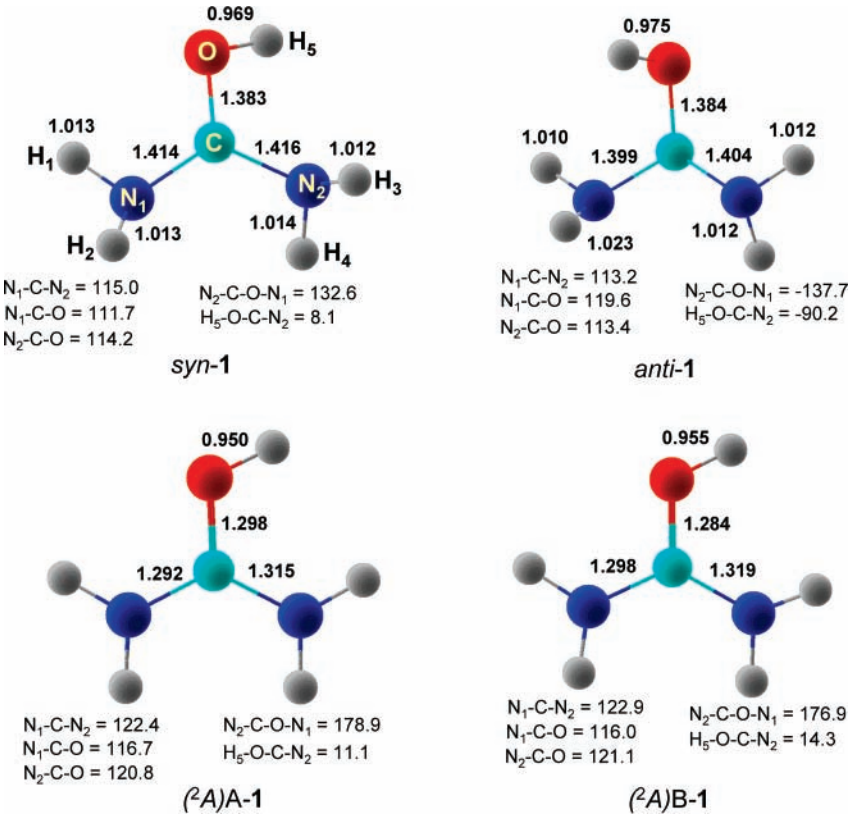

Figure 5. B3LYP/6-311+G(2d,p)-optimized structures of *syn*-**1** and *anti*-**1**, and CIS/6-311++G(2d,p)-optimized structures of A and B excited states of **1**.

TABLE 5: Urea Radical Energies

	relative energy[a,b]			
		B3-PMP2		
species/reaction	B3LYP	A[c]	B[d]	CCSD(T)/aug-cc-pVTZ
syn-**1**	0	0	0	0
syn-**1**(VN)[e]	87	91	91	103
anti-**1**	2.2	2.5	2.4	3.6
TS1	4	4	4	7
TS2	57	57	58	75
TS3	54	55	56	73
4(C_2) + H$^\bullet$	19	5	10	19
4(C_s) + H$^\bullet$	21	6	11	21
anti-syn-**5** + H$^\bullet$	85	70	73	80
anti-anti-**5** + H$^\bullet$	93	78	81	87
syn-anti-**5** + H$^\bullet$	100	86	89	93
syn-syn-**5** + H$^\bullet$	117	101	104	108
TS4a (*anti-syn*)	92	89	90	101
TS4b (*anti-syn*)	93	93	90	101
TS4c (*anti-anti*)	99	94	95	106
TS4d (*syn-anti*)	104	99	101	110
TS6	134	135	133	138
TS7	195	194	193	197
TS8	198	197	195	200
TS9	65	75	74	67
$H_2N-C=O^\bullet + NH_3$	−45	−41	−40	−27
$HN-C-OH^\bullet + NH_3$	42	48	47	54
$NH_2^\bullet + C=O + NH_3$	53	58	58	47

[a] In units of kJ mol^{-1}. [b] Including B3LYP zero-point energies and referring to 0 K. [c] Single-point calculations with the 6-311+G(3df,2p) basis set. [d] Single-point calculations with the aug-cc-pVTZ basis set.

The calculated CCSD(T) transition-state energies were used to obtain unimolecular rate constants by RRKM calculations. The interconversion of *syn*-**1** and *anti*-**1** through **TS1** was fast ($k > 10^{10}$ s^{-1}) and resulted in rapid equilibration. At internal energies above 90 kJ mol^{-1}, which is relevant for radicals formed by vertical electron transfer, both conformers are comparably populated with 42−45% of the less stable *anti*-**1** being present (Figure S3, Supporting Information). The population-weighted rate constants for the H loss through O−H bond dissociation (k_{O-H}) are greater than 10^6 s^{-1} in the entire energy interval above **TS2** and **TS3** and exceed 10^8 s^{-1} for radicals formed by vertical electron transfer with >90 kJ mol^{-1} internal energy (Figure 7). This explains the complete dissociation of **1** on the 4 μs time scale of the $^+NR^+$ experiments. Primary and secondary isotope effects slowed down the dissociation, as shown for the population-weighted RRKM rate constants for H and D losses from **1**-d_1 through **1**-d_5 (Figure S4, Supporting Information). However, the rate constant for the slowest O−D dissociation in **1**-d_5 ($k_{D,O-D}$) was 1.6×10^7 s^{-1} at 90 kJ mol^{-1} internal energy, indicating a negligible fraction of nondissociated **1** after 4 μs. This explains the absence of survivor **1**-d_5^+ in the $^+NR^+$ mass spectrum. The RRKM rate constants for O−H (k_{O-H}) and N−H bond dissociations (k_{N-H}) in *syn*-**1** and the O···H···N migration through **TS6** (k_{O-H-N}) leading to loss of ammonia indicated that in the pertinent range of internal energies *syn*-**1** can be expected to dissociate exclusively by loss of hydroxyl H (Figure S5, Supporting Information). However, the $^+NR^+$ mass spectra of **1**-d_1^+ and **1**-d_4^+ showed losses of H atoms originating from *both* OH and NH_2 groups, which is at variance with the RRKM calculations in Figure S5. Note that the OH and NH_2 hydrogen atoms cannot be scrambled prior to loss of H because the pertinent transition state for O···H···N migration (**TS6**) is above those for O−H and N−H bond dissociations and proceeds to irreversible dissociation by loss of ammonia.

To reconcile the discrepancy between the experiment and RRKM calculations, we considered the formation of excited electronic states upon collisional electron transfer to **1**$^+$. The vertically formed **1** retains the planar geometry of **1**$^+$, which results in 87−103 kJ mol^{-1} vibrational excitation of the (^{2}A)X

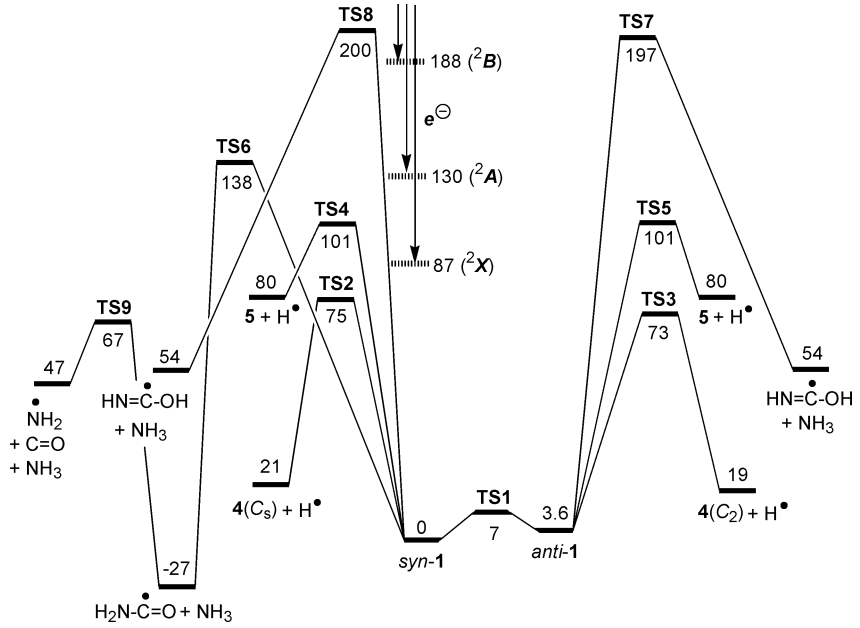

Figure 6. Potential energy scheme for dissociations of *syn*-**1** and *anti*-**1**. The energies are from CCSD(T)/aug-cc-pVTZ single-point calculations and include B3LYP/6-311++G(2d,p) zero-point corrections.

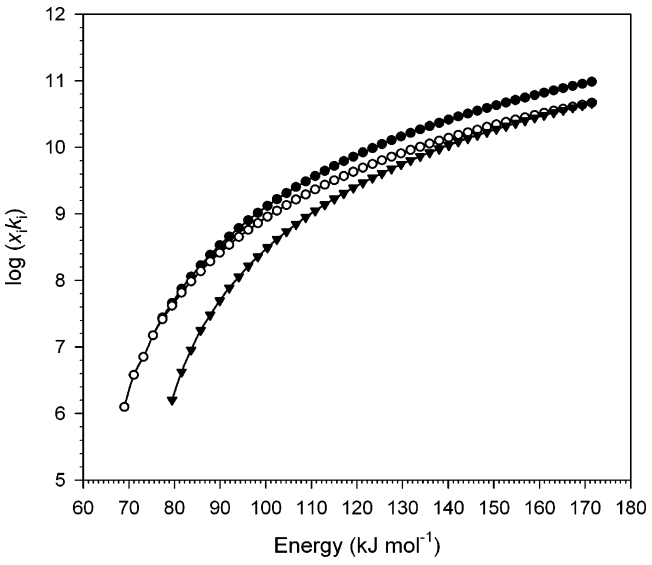

Figure 7. Population-weighted RRKM rate constants (log k, s^{-1}) for O−H bond dissociation in **1**. Open circles, *anti*-**1**; filled triangles, *syn*-**1**; filled circles, total rate constant.

state of **1** due to Franck−Condon effects, as calculated at various levels of theory (Table 5). However, dissociations on the (^{2}A)X state in this energy region should favor O−H bond cleavages. Electron capture in the (^{2}A)A and B states deposits 120−140 and 178−200 kJ mol^{-1}, respectively, in the radical formed, which is sufficient for dissociations by N−H bond cleavages, if the A or B states cross the X state in the vicinity of **TS4** or **TS5**. The (^{2}A)A- and (^{2}A)B-state geometries of radical *syn*-**1** were optimized with CIS/6-311++G(2d,p) and showed near-planar structures that resembled that of $\mathbf{1}^+$ (Figure 5). This indicated that vertical electron transfer to (^{2}A)A and (^{2}A)B states might have substantial cross sections due to favorable Franck−Condon factors and that those states may play a role in the dissociations of *syn*-**1** and *anti*-**1**. Investigation of the potential energy surface of the A and B states was unsuccessful because the CIS calculations oscillated between different electronic states and failed to converge.

Guanidine Ions and Radicals. Protonation of guanidine is expected to occur unequivocally at the imine nitrogen atom to give ion $\mathbf{2}^+$ with a calculated proton affinity of 985 kJ mol^{-1}.[54] The guanidine amino groups are substantially less basic to form cation $\mathbf{8}^+$, which is the less stable tautomer of $\mathbf{2}^+$. Note that the PA of the NH_2 groups in guanidine (846 kJ mol^{-1}) is below that of ammonia (Table 1). The major dissociation of ion $\mathbf{2}^+$ is elimination of ammonia to give the $H_2N-C{=}NH^+$ ion at *m*/*z* 43. The loss of ammonia from $\mathbf{2}^+$ requires 241 kJ mol^{-1} at the thermochemical threshold (Table 3) and likely involves the less stable cation $\mathbf{8}^+$ as an intermediate. The transition state for a $\mathbf{2}^+ \rightarrow \mathbf{8}^+$ isomerization was found at 216 kJ mol^{-1} relative to $\mathbf{2}^+$ (**TS10**, Table 3), which is below the dissociation threshold for the loss of ammonia.

The $^+NR^+$ mass spectrum of $\mathbf{2}^+$ does not show a survivor ion at *m*/*z* 60 (Figure 8a), indicating complete dissociation of the intermediate radical **2** on the 4 μs time scale. The fragments observed in the $^+NR^+$ mass spectrum comprise *m*/*z* 59 (loss of H), *m*/*z* 45−42 (loss of NH_{1-4}), *m*/*z* 29−26 (CNH_{0-3}), *m*/*z* 18 (NH_4^+), and *m*/*z* 15−17 from reionized ammonia. Most of these fragments are also present in the $^+NR^+$ and CAD mass spectra of guanidine cation radical ($\mathbf{9}^{+\bullet}$) and indicate that neutral guanidine (**9**) is one of the dissociation products of radical **2** (Figure 8c). The survivor ion was also absent in the NR mass spectrum of **2**-d_6^+ (Figure 8b), which showed fragments at *m*/*z* 64 (loss of D), *m*/*z* 48 (loss of ND_2), *m*/*z* 46 (loss of ND_3), *m*/*z* 26−30, 22 (ND_4^+), 20 ($ND_3^{+\bullet}$), and 18 (ND_2^+).

The main dissociations of radical **2** were addressed by calculations of the pertinent energies for transition states, intermediates, and products, as summarized in Table 6. Radical **2** was found to have three rotamers of very similar free energies (**2a**, **2b**, and **2c**, Figure 9) that coexist at 298 K equilibrium. All three rotamers of **2** are pyramidized at the central C atom,[55] which contrasts the planar C_3 geometry of the precursor ion $\mathbf{2}^+$.[54] Another structural difference between **2a**−**2c** and $\mathbf{2}^+$ is the N−C bond lengths, which are substantially greater in the radicals (1.404−1.431 Å) than in the ion (1.337 Å). Consequently, vertical electron transfer to $\mathbf{2}^+$ is accompanied by Franck−Condon effects that result in a 81−126 kJ mol^{-1} vibrational excitation in the **2** formed. The broad range of the

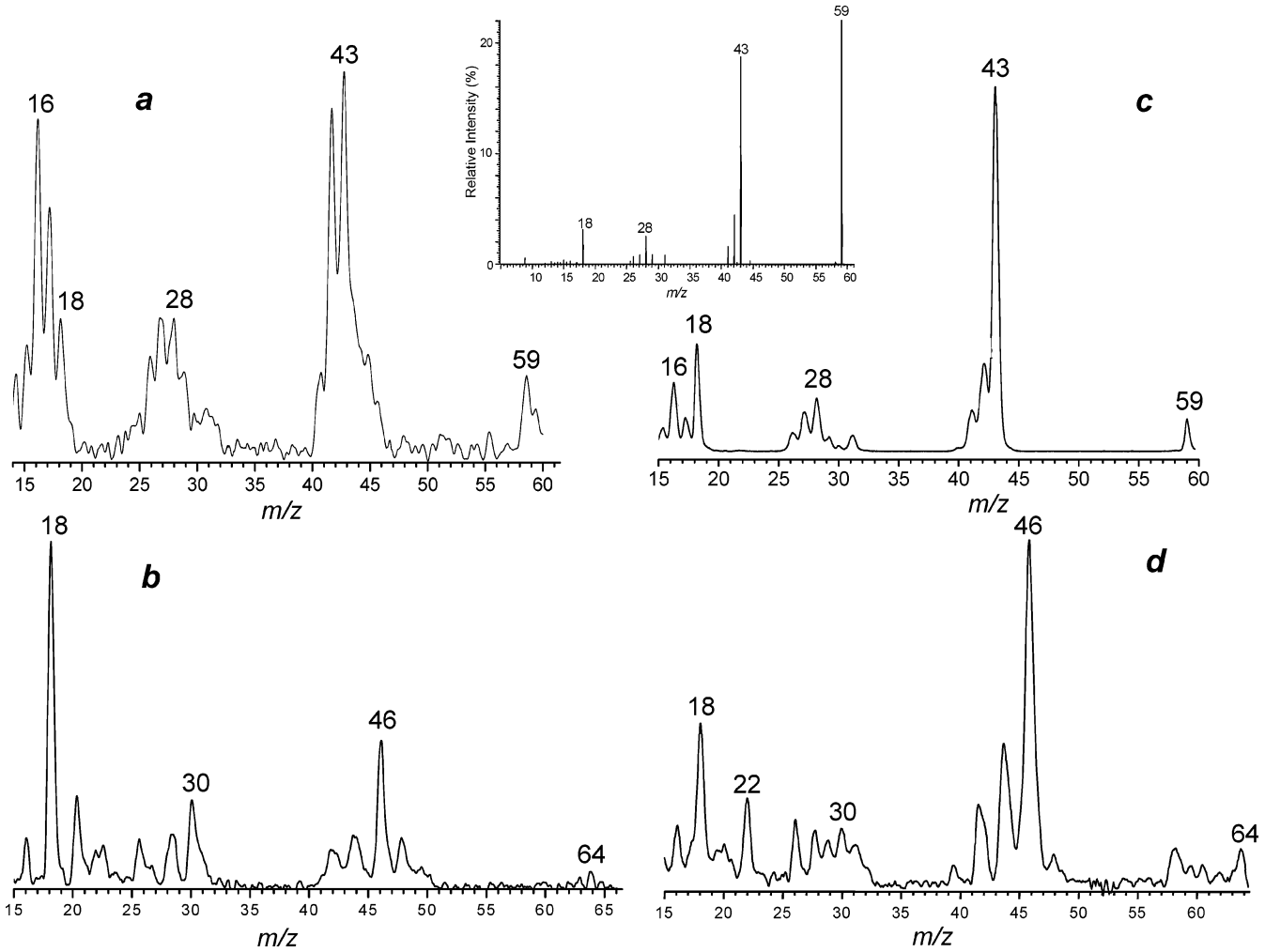

Figure 8. $^{+}NR^{+}$ mass spectra (CH_3SSCH_3, 70% transmittance/O_2, 70% transmittance) of (a) $\mathbf{2}^{+}$ (b) $\mathbf{2}$-d_6^{+}, (c) $\mathbf{9}^{+\bullet}$, and (d) $\mathbf{9}$-$d_5^{+\bullet}$. Inset shows the CAD/He spectrum of $\mathbf{9}^{+\bullet}$.

TABLE 6: Guanidine Radical Energies

	relative energy[a,b]			
		B3-PMP2		
species/reaction	B3LYP	A[c]	B[d]	CCSD(T)/ aug-cc-pVTZ
2a	0	0	0	0
2b	1.8	1.1	1.0	0.7 (−0.7)[e]
2c	3.3	4.6	4.6	6.2 (5.8)[e]
2(VN)	81	89	85	126
8	143	155	144	149
2a → **9** + H	98	74	77	82
2a → **TS11**	92	86	89	104
2a → **TS12**	146	166	160	158
2a → $H_2N-C-NH_2 + NH_2^{\bullet}$	157	170	169	166
2a → $H_2N-C=NH^{\bullet} + NH_3$	53	50	50	60
10	143	155	159	155

[a] In units of kJ mol^{-1}. [b] Including B3LYP zero-point energies and referring to 0 K. [c] Single-point calculations with the 6-311+G(3df,2p) basis set. [d] Single-point calculations with the aug-cc-pVTZ basis set. [e] $\Delta G^{\circ}_{g,298}$ values.

calculated Franck−Condon energies reflects the spread in the single-point energies obtained by different methods.

The minimum-energy dissociation of **2a** was loss of one of the hydrogen atoms to form guanidine, which required 82 kJ mol^{-1} at the thermochemical threshold. The B3LYP potential energy surface showed a continuously endothermic dissociation (Figure S6, Supporting Information). However, both B3-PMP2 and CCSD(T) single-point energy calculations found a potential energy maximum that was fitted to locate the transition state (**TS11**) at d(N−H) = 1.56 Å, which was 86−104 kJ mol^{-1} above **2** at different levels of theory. Note that the **TS11** energy was close to the Franck−Condon energy gained upon vertical electron transfer, indicating that radicals **2** had sufficient internal energy to dissociate upon formation. This was consistent with the absence of survivor ion in the $^{+}NR^{+}$ mass spectrum of $\mathbf{2}^{+}$.

Loss of ammonia from **2a** was calculated to require only 60 kJ mol^{-1} at the thermochemical threshold and can proceed by two different pathways. One is a rearrangement by H-atom migration to form the high-energy isomer **8** at 149 kJ mol^{-1} above **2a**. Since **8** is a local energy minimum, it must be separated from both **2a** and the dissociation products by additional energy barriers at >150 kJ mol^{-1} above **2a**. An alternative pathway to elimination of ammonia is by C−N bond dissociation in **2a** through **TS12** leading to an $H_2N\cdots H_2N-C-NH_2$ dipole−dipole complex (**10**) in which the NH_2 radical can exothermically abstract a hydrogen atom to form ammonia (Scheme 4). However, this pathway requires a TS energy ($E_{\mathbf{TS12}}$ = 158 kJ mol^{-1} relative to **2a**) that is considerably greater than that for loss of H, and thus the latter dissociation should be kinetically more favorable in the ground electronic state of **2a**.

The electronic states of vertically formed **2** consist of Rydberg-like 3s (X), 3p (B, C), and 3d (D, E) states and a π^* state (A) (Figure S7, Supporting Information) The degenerate D and E states have sufficient internal energy (85 + 136 = 221 kJ mol^{-1}), radiative lifetime (5.6 μs), and nodal properties

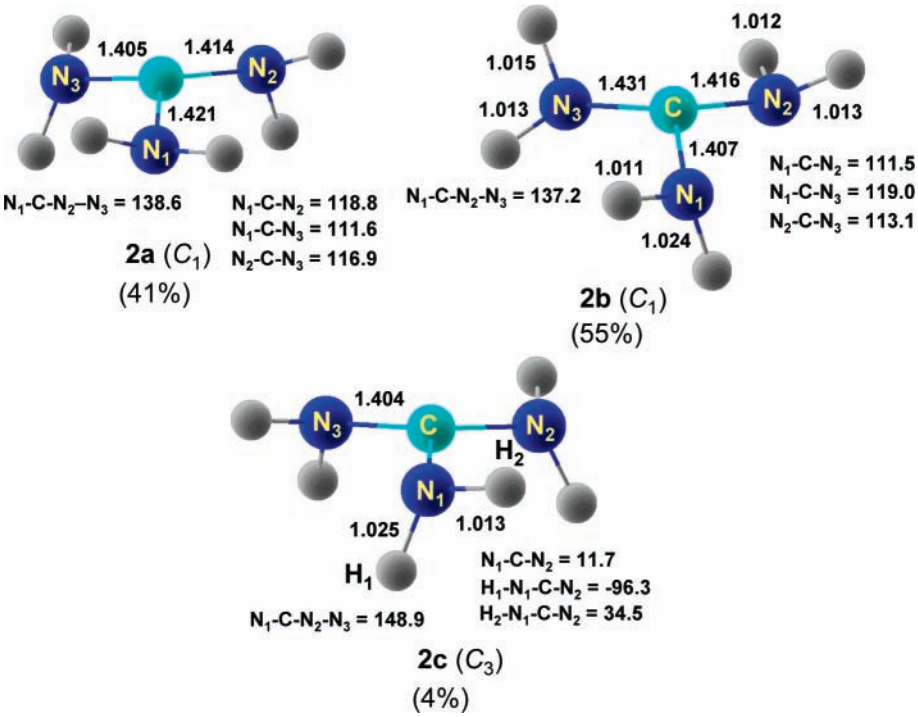

Figure 9. B3LYP/6-31++G(d,p)-optimized structures of **2a**−**2c**.

SCHEME 4

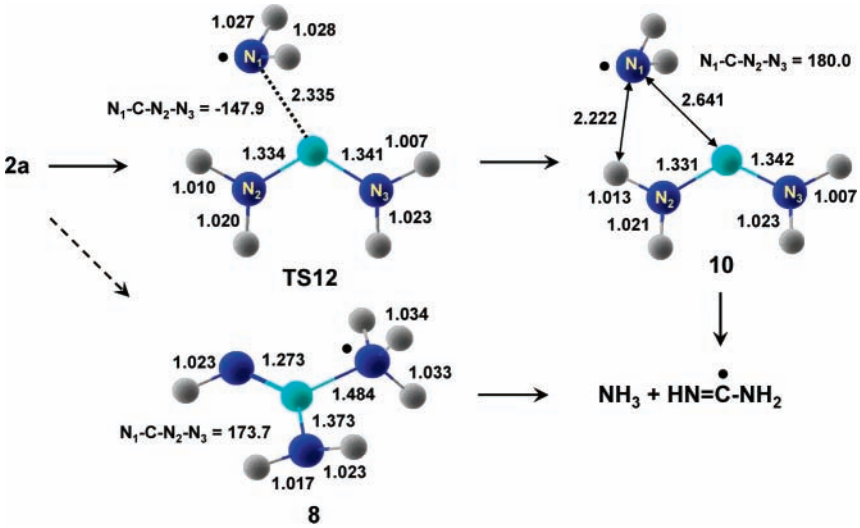

to participate in the loss of NH_2 and NH_3. Hence, in light of the energy data, it appears that the fragments observed in the $^{+}NR^{+}$ mass spectrum of $\mathbf{2}^{+}$ are formed by combination of H loss from the ground state of **2**, NH_2 and NH_3 losses from the excited states of **2**, and post-reionization dissociations of cation radical $\mathbf{9}^{+\bullet}$. The dissociation energies of $\mathbf{9}^{+\bullet}$ are summarized in Table 4.

Radical Stabilities. How does multiple substitution by π-donating amino groups affect the radical stabilities? To address this question, we calculated the reaction enthalpies for isodesmic H-atom exchange between methane and methyl radicals carrying one to three NH_2 groups (Table 7). The presence of one amino group results in a 47 kJ mol^{-1} decrease in the C−H bond dissociation energy in CH_3NH_2 relative to methane, which can be ascribed to the stabilization of the aminomethyl radical through three-electron interaction between the C and N 2p atomic orbitals.[5,7] Addition of a second amino group in $CH_2(NH_2)_2$ results in a further albeit substantially smaller decrease of the C−H bond dissociation energy to −54 kJ mol^{-1} relative to that in methane. The third amino group in

TABLE 7: Isodesmic Reaction Enthalpies for Amine-Substituted Methyl Radicals

	relative energy[a,b]				
			B3-PMP2		
reaction	B3LYP	G2(MP2)	A[c]	B[d]	CCSD(T)/aug-cc-pVTZ
2a + CH_4 → $HC(NH_2)_3 + CH_3^{\bullet}$	74	55	64	63	54 (378)[e]
$HC^{\bullet}(NH_2)_2 + CH_4$ → $H_2C(NH_2)_2 + CH_3^{\bullet}$	66	55	61	61	54 (378)[e]
$H_2C^{\bullet}-NH_2 + CH_4$ → $H_3C-NH_2 + CH_3^{\bullet}$	56	48	52	52	47 (385)[e]

[a] In units of kJ mol^{-1}. [b] Including B3LYP/6-31+G(d,p) zero-point corrections and referring to 0 K. [c] Single-point calculations with the 6-311+G(3df,2p) basis set. [d] Single-point calculations with the aug-cc-pVTZ basis set. [e] C−H bond dissociation energies based on the BDE in methane (432 kJ mol^{-1}).[57]

TABLE 8: Ionization Energies of Substituted Methyl Radicals

	ionization energy[a,b]				
			B3-PMP2		CCSD(T)/
radical	B3LYP	G2(MP2)	A[c]	B[d]	aug-cc-pVTZ
$C(OH)_3^{\bullet}$	6.04	5.82	5.85	5.88	5.88
$C(OH)_2NH_2^{\bullet}$	5.35	5.18	5.19	5.23	5.24
$C(OH)(NH_2)_2^{\bullet}$ (**1**)	4.83	4.69	4.64	4.67	4.75
$CH_2NH_2^{\bullet}$	6.39	6.16	6.30	6.33	6.23
$CH(NH_2)_2^{\bullet}$	4.93	4.83	4.85	4.89	4.89
$C(NH_2)_3^{\bullet}$ (**2a**)	4.33	4.23	4.20	4.24	4.29

[a] Adiabatic ionization energies in units of electronvolts. [b] Including B3LYP/6-31+G(d,p) zero-point corrections and referring to 0 K. [c] Single-point calculations with the 6-311+G(3df,2p) basis set. [d] Single-point calculations with the aug-cc-pVTZ basis set.

$HC(NH_2)_3$ has a negligible effect on the C−H bond dissociation energy, which is practically identical to that in $CH_2(NH_2)_2$. Hence, one can conclude that the radical stabilization in **2a** is quantitatively similar to that in the other amino-substituted methyl radicals.

Ionization Energies. The hydroxyl and amino groups are π-electron-donating and σ-electron-withdrawing substituents that affect the electron density at the carbon atom in substituted methyl radicals. This combined effect results in a moderate stabilization of the radicals, as discussed above. A larger effect is observed on the corresponding cations, which are stabilized by π-electron donation of the OH and NH_2 groups.[7] This effect is reflected by the very low ionization energies of OH- and NH_2-substituted radicals.[3] The calculated adiabatic ionization energies of a series of substituted methyl radicals, e.g., $C(OH)_3$, $C(OH)_2NH_2$, **1**, CH_2NH_2, $CH(NH_2)_2$, and **2a**, are collated in Table 8. The data indicate that the amino groups have a major effect on the ionization energies. Replacing hydrogen atoms in methane by NH_2 groups results in a large decrease of radical ionization energies, e.g., from 9.84 eV in the methyl radical[52] to 6.32, 4.89, and 4.29 eV in CH_2NH_2, $CH(NH_2)_2$, and **2a**, respectively. Replacing the weaker π-donating and stronger σ-withdrawing OH groups with NH_2 decreases the IE by 0.64, 0.49, and 0.46 eV from $C(OH)_3$ to $C(OH)_2NH_2$, **1**, and **2a**, respectively. The IE of **1** (4.75 eV) is below that of Na, and the IE of **2a** (4.29 eV) is between those of K and Rb, justifying the term "organic alkali metal" for both radicals.

The decrease in the electron binding energy does not correlate with the radical stabilities if the latter are expressed by the C−H bond energies (Table 7). This is understandable from the molecular orbital representation of the π-type interactions in CH_2NH_2, $CH(NH_2)_2$, and **2a** (Figure S8, Supporting Information). In each case, the interaction between the carbon and nitrogen 2p atomic orbitals results in highest singly occupied molecular orbitals (SOMOs) of a $[2p(C) - \sum 2p(N_{1-3})]$ type that have nodal planes dissecting the C−N bonds and whose energies increase with the number of antibonding π-interactions. This qualitatively explains the decreasing ionization energies in the CH_2NH_2, $CH(NH_2)_2$, **2a** series. The underlying doubly occupied molecular orbitals are of two types. The first type is MOs formed by antibonding combinations of 2p(N) atomic orbitals whose energies slightly decrease with the number of N atoms. The other type comprises bonding π(C−N) orbitals that are combined in a bonding or antibonding sense with 2p(N) atomic orbitals on the remaining N atoms. These orbital energies slightly increase with the number of nitrogen atoms. The combined effects on orbital energies of the 2p(C) and 2p(N) interactions roughly cancel out, resulting in a comparable but moderate overall stabilization for all aminomethyl radicals, as obtained quantitatively from ab initio calculations.

Conclusions

Diaminohydroxymethyl and triaminomethyl radicals represent electron super-rich species that were transiently generated in the gas phase by femtosecond collisional electron transfer. The differences between the precursor cation and radical geometries resulted in vibrational excitation through Franck−Condon effects and formation of excited electronic states. The combined effect of excitation upon electron transfer was fast dissociation of the radicals by loss of hydrogen atoms and C−N bond cleavages. Ab initio calculations showed that the π-electron-donating NH_2 groups have a moderate effect on increasing the radical stabilities and a major effect on decreasing the electron binding energies.

Acknowledgment. Support of this work by the National Science Foundation (Grant CHE-0349595 for experiments and Grant CHE-0342956 for computations) is gratefully acknowledged. The Computational Chemistry Center at the UW Department of Chemistry receives joint support from the NSF and the University of Washington. Thanks are due to Dr. Martin Sadilek for technical assistance with mass spectra measurements. The JEOL HX-110 mass spectrometer was a generous donation from the former Seattle Biomembrane Institute by courtesy of Prof. S. Hakomori.

Supporting Information Available: Figures S1−S8 with auxiliary $^{+}NR^{+}$ mass spectra, B3LYP/6-311++G(2d,p)-optimized structures, RRKM rate constants, potential energy surfaces, and excited-state energies and molecular orbitals. This material is available free of charge via the Internet at http://pubs.acs.org.

References and Notes

(1) Sana, M.; Leroy, G.; Peeters, D.; Younang, E. *THEOCHEM* **1987**, *36*, 325−330.
(2) Leroy, G.; Sana, M.; Wilante, C. *THEOCHEM* **1991**, *74*, 37−45.
(3) Griller, D.; Lossing, F. P. *J. Am. Chem. Soc.* **1981**, *103*, 1586−1587.
(4) Clark, K. B.; Wayner, D. D. M. *J. Am. Chem. Soc.* **1991**, *113*, 9363−9365.
(5) Henry, D. J.; Parkinson, C. J.; Mayer, P. M.; Radom, L. *J. Phys. Chem. A* **2001**, *105*, 6750−6756.
(6) Wood, G. P. F.; Moran, D. Jacob, R.; Radom, L. *J. Phys. Chem. A* **2005**, *109*, 6318−6325.
(7) Lalevee, J.; Allonas, X.; Fouassier, J.-P. *J. Am. Chem. Soc.* **2002**, *124*, 9613−9621.
(8) Shaffer, S. A.; Tureček, F.; Cerny, R. L. *J. Am. Chem. Soc.* **1993**, *115*, 12117−12124.
(9) Tureček, F. *Top. Curr. Chem.* **2003**, *225*, 77−129.
(10) Zubarev, R. A.; Kelleher, N. L.; McLafferty, F. W. *J. Am. Chem. Soc.* **1998**, *120*, 3265−3266.
(11) (a) Coon, J. J.; Ueberheide, B.; Syka, J. E. P.; Dryhurst, D. D.; Ausio, J.; Shabanowitz, J.; Hunt, D. F. *Proc. Natl. Acad. Sci. U.S.A.* **2005**, *102*, 9463−9468. (b) Pitteri, S. J.; Chrisman, P. A.; Hogan, J. M.; McLuckey, S. A. *Anal. Chem.* **2005**, *77*, 1831−1839. (c) Xia, Y.; Chrisman, P. A.; Pitteri, S. J.; Erickson, D. E.; McLuckey, S. A. *J. Am. Chem. Soc.* **2006**, *128*, 11792−11798.
(12) Tureček, F.; Syrstad, E. A. *J. Am. Chem. Soc.* **2003**, *125*, 3353−3369.
(13) Syrstad, E. A.; Tureček, F. *J. Phys. Chem. A* **2001**, *105*, 11144−11155.
(14) Syrstad, E. A.; Stephens, D. D.; Tureček, F. *J. Phys. Chem. A* **2003**, *107*, 115−126.
(15) Tureček, F. *J. Am. Chem. Soc.* **2003**, *125*, 5954−5963.
(16) Tam, F.; Syrstad, E. A.; Chen, X.; Tureček, F. *Eur. J. Mass Spectrom.* **2004**, *10*, 869−879.
(17) *CRC Handbook of Physics and Chemistry*, 87th ed.; Lide, Ed.; CRC Press: Boca Raton, FL, 2006; p 10-202.
(18) Wohler, F. *Poggendorff's Ann. Phys.* **1828**, *12*, 253−256.

(19) Duvernay, F.; Chiavassa, F.; Borget, F.; Aycard, J.-P. *J. Phys. Chem. A* **2005**, *109*, 6008−6018.
(20) Beddie, C.; Webster, C. E.; Hall, M. B. *Dalton Trans.* **2005**, 3542−3551.
(21) Estiu, G. L.; Merz, K. M. *J. Am. Chem. Soc.* **2004**, *126*, 6932−6944.
(22) Estiu, G. L.; Merz, K. M. *J. Am. Chem. Soc.* **2004**, *126*, 11832−11842.
(23) Barrios, A. M.; Lippard, S. J. *J. Am. Chem. Soc.* **2000**, *122*, 9172−9177.
(24) Tsipis, C. A.; Karipidis, P. A. *J. Am. Chem. Soc.* **2003**, *125*, 2307−2318.
(25) Schaber, P. M.; Colson, J.; Higgins, S.; Thielen, D.; Anspach, B.; Brauer, J. *Thermochim. Acta* **2004**, *424*, 131−142.
(26) Yim, S. D.; Kim, S. J.; Baik, J. H.; Nam, I.-S.; Mok, Y. S.; Lee, J.-H.; Cho, B. K.; Oh, S. H. *Ind. Eng. Chem. Res.* **2004**, *43*, 4856−4863.
(27) Rasul, G.; Prakash, G. K. S.; Olah, G. A. *J. Org. Chem.* **1994**, *59*, 2552−2556.
(28) Notario, R.; Catsano, O.; Herreros, M.; Abboud, J.-L. M. *THEOCHEM* **1996**, *371*, 21−29.
(29) Del Bene, J. E.; Radovick, S. *J. Am. Chem. Soc.* **1978**, *100*, 6936−6941.
(30) Wen, N.; Brooker, M. H. *J. Phys. Chem.* **1993**, *97*, 8608−8616.
(31) Wang, F.; Ma, S.; Zhang, D.; Cooks, R. G. *J. Phys. Chem. A* **1998**, *102*, 2988−2994.
(32) Zheng, X.; Cooks, R. G. *J. Phys. Chem. A* **2002**, *106*, 9939−9946.
(33) Harkema, S.; Feil, D. *Acta Crystallogr.* **1969**, *B25*, 589−591.
(34) (a) Hall, N. F.; Sprinkle, M. R. *J. Am. Chem. Soc.* **1932**, *54*, 3469−3485. (b) Angyal, S. J.; Warburton, W. K. *J. Chem. Soc.* **1951**, 2492−2494. (c) Perrin, D. D. *Dissociation Constants of Organic Bases in Aqueous Solution*; Butterworths: London, 1965; p 444.
(35) Shi, T.; Zhao, J.; Shek, P. Y. I.; Hopkinson, A. C.; Siu, K. W. M. *Can. J. Chem.* **2005**, *83*, 1941−1952.
(36) Turecek, F.; Gu, M.; Shafer, S. A. *J. Am. Soc. Mass Spectrom.* **1992**, *3*, 493−501.
(37) Turecek, F. *Org. Mass Spectrom.* **1992**, *27*, 1087−1097.
(38) Frisch, M. J.; Trucks, G. W.; Schlegel, H. B.; Scuseria, G. E.; Robb, M. A.; Cheeseman, J. R.; Montgomery, J. A., Jr.; Vreven, T.; Kudin, K. N.; Burant, J. C.; Millam, J. M.; Iyengar, S. S.; Tomasi, J.; Barone, V.; Mennucci, B.; Cossi, M.; Scalmani, G.; Rega, N.; Petersson, G. A.; Nakatsuji, H.; Hada, M.; Ehara, M.; Toyota, K.; Fukuda, R.; Hasegawa, J.; Ishida, M.; Nakajima, T.; Honda, Y.; Kitao, O.; Nakai, H.; Klene, M.; Li, X.; Knox, J. E.; Hratchian, H. P.; Cross, J. B.; Adamo, C.; Jaramillo, J.; Gomperts, R.; Stratmann, R. E.; Yazyev, O.; Austin, A. J.; Cammi, R.; Pomelli, C.; Ochterski, J. W.; Ayala, P. Y.; Morokuma, K.; Voth, G. A.; Salvador, P.; Dannenberg, J. J.; Zakrzewski, V. G.; Dapprich, S.; Daniels, A. D.; Strain, M. C.; Farkas, O.; Malick, D. K.; Rabuck, A. D.; Raghavachari, K.; Foresman, J. B.; Ortiz, J. V.; Cui, Q.; Baboul, A. G.; Clifford, S.; Cioslowski, J.; Stefanov, B. B.; Liu, G.; Liashenko, A.; Piskorz, P.; Komaromi, I.; Martin, R. L.; Fox, D. J.; Keith, T.; Al-Laham, M. A.; Peng, C. Y.; Nanayakkara, A.; Challacombe, M.; Gill, P. M. W.; Johnson, B.; Chen, W.; Wong, M. W.; Gonzalez, C.; Pople, J. A. *Gaussian 03*, revision B.05; Gaussian, Inc.: Pittsburgh, PA, 2003.
(39) (a) Becke, A. D. *J. Chem. Phys.* **1993**, *98*, 1372−1377. (b) Becke, A. D. *J. Chem. Phys.* **1993**, *98*, 5648−5652. (c) Stephens, P. J.; Devlin, F. J.; Chabalowski, C. F.; Frisch, M. J. *J. Phys. Chem.* **1994**, *98*, 11623−11627.
(40) Rauhut, G.; Pulay, P. *J. Phys. Chem.* **1995**, *99*, 3093−3100.
(41) Dunning, T. H., Jr. *J. Chem. Phys.* **1989**, *90*, 1007−1023.
(42) Pople, J. A; Head-Gordon, M.; Raghavachari, K. *J. Chem. Phys.* **1987**, *87*, 5968−5975.
(43) Čížek, J.; Paldus, J.; Šroubková, L. *Int. J. Quantum Chem.* **1969**, *3*, 149−167.
(44) Purvis, G. D.; Bartlett, R. J. *J. Chem. Phys.* **1982**, *76*, 1910−1918.
(45) Tureček, F.; Polášek, M.; Frank, A. J.; Sadílek, M. *J. Am. Chem. Soc.* **2000**, *122*, 2361−2370.
(46) Stratmann, R. E.; Scuseria, G. E.; Frisch, M. J. *J. Chem. Phys.* **1998**, *109*, 8218−8224.
(47) Foresman, J. B.; Head-Gordon, M.; Pople, J. A.; Frisch, M. J. *J. Phys. Chem.* **1992**, *96*, 135−149.
(48) Gilbert, R. G.; Smith, S. C. *Theory of Unimolecular and Recombination Reactions*; Blackwell Scientific Publications: Oxford, 1990; pp 52−132.
(49) Zhu, L.; Hase, W. L. *Quantum Chemistry Program Exchange*; Indiana University: Bloomington, 1994; Program No. QCPE 644.
(50) Frank, A. J.; Sadílek, M.; Ferrier, J. G.; Tureček, F. *J. Am. Chem. Soc.* **1997**, *119*, 12343−12353.
(51) Chen, X.; Syrstad, E. A.; Gerbaux, P.; Nguyen, M. T.; Tureček, F. *J. Phys. Chem. A* **2004**, *108*, 9283−9293.
(52) Standard Reference Database No. 69, March 2003 Release; http://webbook.nist.gov/chemistry.
(53) (a) Syrstad, E. A.; Vivekananda, S.; Tureček, F. *J. Phys. Chem. A* **2001**, *105*, 8339−8351. (b) Wolken, J. K.; Tureček, F. *J. Phys. Chem. A* **2001**, *105*, 8352−8360.
(54) For previous computational studies of guanidine cations, see: (a) Peeters, D.; Leroy, G.; Wilante, C. *J. Mol. Struct.* **1997**, *416*, 21−32. (b) Maksic, Z. B.; Kovacevic, B. *J. Phys. Chem. A* **1998**, *102*, 7324−7328. (c) Kovacevic, B.; Maksic, Z. B. *Chem.—Eur. J.* **2002**, *8*, 1694−1702. (d) Kovacevic, B.; Maksic, Z. B.; Vianello, R. *J. Chem. Soc., Perkin Trans. 2* **2001**, 886−891. (e) Gobbi, A.; Frenking, G. *J. Am. Chem. Soc.* **1993**, *115*, 2362−2372.
(55) For previous computational studies involving guanidine radicals, see: (a) Feuerbacher, S.; Santra, R. *J. Chem. Phys.* **2005**, *123*, 194310/1-8. (b) Albert, K.; Roesch, N. *Chem. Ber.* **1997**, *130*, 1745−1749. (c) Berges, J.; Abedinzadeh, Z.; Houee-Levin, C.; Conte, D.; Langlet, J.; Kassab, E. *J. Chim. Phys. Biol.* **1996**, *93*, 7−11.
(56) Curtiss, L. A.; Raghavachari, K.; Pople, J. A. *J. Chem. Phys.* **1993**, *98*, 1293−1298.
(57) Partridge, H.; Bauschlicher, C. W., Jr. *J. Chem. Phys.* **1995**, *103*, 10589−10596.